Physics – Uspekhi **67** (5) 464 – 486 (2024)

REVIEW OF TOPICAL PROBLEMS

PACS numbers: 52.25.Xz, **52.55. – s,** 52.80.Sm

Generation of a radial electric field in a cylindrical plasma column with an axial magnetic field

G D Liziakin, A V Gavrikov, S D Kuzmichev, V P Smirnov, R A Usmanov

DOI: https://doi.org/10.3367/UFNe.2023.12.039622

Contents

Abstract. The current state of research on generating and controlling a radial electric field in a magnetized plasma in cylindrical geometry is reviewed. Such systems are widely used in many plasma-physics applications ranging from thermonuclear fusion and plasma mass separation to the development of plasma thrusters. Primarily experimental studies are analyzed with an emphasis on the installation parameters and experiments conditions that enable generating controlled distributions of electrical potential. Data reported by various research teams are summarized in tables, allowing predictions of the potential reproducible under specific experimental conditions.

Keywords: biased electrodes, electric potential control, perpendicular electric field, electric field in plasma, magnetized plasma, plasma mass separation, open traps, Penning discharge

1. Introduction

In the last two decades, interest has rekindled in the mass separation of charged particles using plasma methods [1, 2]. These methods have turned out to be applicable in several areas, including reprocessing of spent nuclear fuel [3–9], recycling of rare earth elements [10], isotope separation [11–13], and reprocessing of nuclear waste [14]. A distinctive feature of plasma methods from electromagnetic separation in a vacuum is that the separated flow moves under conditions of compensated space charge, enabling a significant enhancement of productivity and, consequently, reduction in energy costs.

The schemes proposed in [1, 2] include those [4, 9, 15–17] in which the trajectories of separated particles depend on the distribution of the electric field. Due to this circumstance, there are several urgent issues: Is it possible to control the electric potential in a plasma? In what range and under what parameters is such control possible? What is the maximum accuracy of setting a given electric potential profile? These issues are of importance not only in relation to plasma methods for mass separation but also in such areas as open systems for thermonuclear fusion, electric propulsion thrusters, and plasma sources.

The feasibility of creating a stationary distribution of electric potential inside a plasma volume requires some clarification. It is well known that, when an electrode with a potential different from that of space is immersed in a quasi-neutral plasma, a sheath of space charge is formed near the electrode, which screens the main volume of the quasi-neutral plasma from the electrode potential [18, 19]. Generally speaking, the structure of the space charge layer can be quite complex [20], but the existence of the screening effect intuitively suggests that special conditions are needed to create stationary electric fields in the plasma. One of these essential conditions is that the plasma be placed in an external stationary magnetic field, where the motion of charged particles becomes anisotropic.

If electrons are magnetized, their mobility along magnetic field lines is much greater than in the transverse direction. As a result, due to high conductivity, the plasma potential along the magnetic field lines changes insignificantly, and lines become equipotential [21]. At the same time, the transport of electrons across the magnetic field is restricted, and if an electric voltage is applied to two electrodes through which different magnetic field lines pass, a potential difference arises between these lines. It

G D Liziakin [(a)], **A V Gavrikov** [(b)], **S D Kuzmichev** [(c)], **V P Smirnov** [(d)], **R A Usmanov** [(e)]
Joint Institute for High Temperatures, Russian Academy of Sciences, ul. Izhorskaya 13, str. 2, 125412 Moscow, Russian Federation
E-mail: [(a)] glizyakin@gmail.com, [(b)] gavrikov@ihed.ras.ru, [(c)] sdkuzmichev@gmail.com, [(d)] vpsmirnov@rosatom.ru, [(e)] usmanov.r@ihed.ras.ru

Received 23 May 2023, revised 5 December 2023
Uspekhi Fizicheskikh Nauk **194** (5) 495 – 519 (2024)
Translated by M Zh Shmatikov

exists not only in the near-electrode layers but also in the entire volume of the plasma. In this way, a system of crossed stationary electric and magnetic fields is formed.

Experiments show that the above consideration is highly idealized. In reality, for example, to control the radial distribution of the electric potential in a plasma in a cylindrically symmetric geometry, it is necessary to take into account many other parameters of the system (location, geometry and material of electrodes, background gas pressure, etc.) apart from the electron magnetization factor. We discuss in this review examples of the experimentally established influence of various system parameters on the features of the electric field created in a magnetized plasma.

In the configuration of crossed electric **E** and magnetic **B** fields, charged particles drift in the $\mathbf{E} \times \mathbf{B}$ direction. We limit our consideration by only considering systems with cylindrical symmetry, in which a closed drift of particles is realized. The entire class of devices using the crossed-field configuration can be divided into those where the plasma is created only due to the voltage applied to the electrodes and devices where the plasma is created due to additional ionization sources, while the electrodes only vary the plasma potential. The fundamental difference between these classes of devices is that the latter, apparently, are more promising with regard to the possibility of independent control of plasma parameters such as density, temperature, and spatial distribution of the electric field.

The first type of device includes [22], for example, a reflex discharge, a flat magnetron, a cylindrical magnetron, Hall effect engines, and some types of plasma centrifuges. The second type of device is more difficult to characterize by a specific type of discharge. They are devices intended for various purposes and usually have a cylindrical vacuum chamber and a longitudinal magnetic field. They are used, for example, for research in mass separation and magnetic plasma confinement.

Initially, the study of such devices only consisted in measuring I-V curves as a function of the magnetic field and gas pressure. However, as early as 1970, it became clear that integral characteristics are not sufficient to describe the discharge [23]. The spatial distribution of fields and particles, the distribution of particle velocities, and their influence on the excitation of plasma instabilities should also be measured. In practice, such measurements are very difficult. The necessary information can be partially obtained using computer simulation. A common technique for modeling plasma devices in crossed $\mathbf{E} \times \mathbf{B}$ fields is the particle-in-cell (PIC) method. Today, computer programs use up to a thousand cores [24] and make it possible to calculate plasma objects with characteristic dimensions of 10^{-2} m with a particle density on the order of 10^{17} m^{-3}, but for the most part in only 2D geometry [25]. To boost calculations, the gyrokinetic approximation [26], various hybrid models [27], and scaling rules [28, 29] are used. In the last few years, joint efforts of several laboratories resulted in the calculation of the same system using seven independent programs, thereby provided a 'reference' example (benchmark) [24, 30] in this area of research.

Despite recent successes, modeling does not provide an understanding of all the issues pertaining to the physics of rotating plasma, and calculations even for fairly simple geometries turn out to be extremely resource intensive. The study of systems in crossed $\mathbf{E} \times \mathbf{B}$ fields is complicated by the occurrence of instabilities [31] and the phenomenon of anomalous electron transport across the magnetic field [32–34]. The complexity of correctly modeling complex systems of larger dimensions in some cases is comparable to that of conducting real experiments. As a result, researchers often reduce models to identify dominant mechanisms [35]. There are also simplified models, which provide an explanation of experimental results at a qualitative level [36, 37].

Thus, today, to describe and predict plasma processes that occur in large installations, it is necessary to use the data gained from theoretical, computational and experimental studies. The purpose of this review is to summarize the experimental experience gained in creating a radial electric field in plasma systems with an axial magnetic field. The emphasis is done on the experimental setup and the main results pertaining to the creation of a controlled radial distribution of the electric potential in the plasma volume. It should be stressed that the review focuses primarily on the results achieved and bypasses a comprehensive discussion of the complex physical nature of the processes that arise in each specific case. Readers interested in a deeper and more comprehensive understanding of these issues are referred to, for example, reviews [25, 38, 39].

At the beginning of the review, general features of plasma systems in crossed $\mathbf{E} \times \mathbf{B}$ fields are considered; the typical geometry of experimental setups is described, and the parameters that determine the generated electric field in the plasma volume are listed. Next, we consider studies devoted to the generation of a radial electric field in self-sustained Penning discharges, which are explored both per se and as a technique for plasma confinement in open traps. Then, plasma systems in crossed $\mathbf{E} \times \mathbf{B}$ fields with additional (apart from the electrodes that set the electric potential) ionizers of various types are considered. Heated surfaces (Q-machines), microwave sources, RF discharges, and emitters of charged particles, represented by both thermionic electron emitters and plasma beam emitters can be used as such ionizers. These systems are now widely applied for the same problems of plasma confinement and plasma mass separation. The main experimental data obtained in the studies reviewed are collected in tables, which enable, based on the experimental parameters, predicting what electric fields and electric potential amplitudes can, in principle, be reproduced under specific conditions.

2. General scheme of axisymmetric plasma systems with crossed $\mathbf{E} \times \mathbf{B}$ fields and their features

Most of the experimental apparatuses reviewed here feature a cylindrical geometry and symmetry with respect to the system axis. Figure 1 shows a general setup of such axisymmetric plasma systems with crossed $\mathbf{E} \times \mathbf{B}$ fields.

The apparatus is usually a cylindrical vacuum chamber, which in most cases is grounded. The chamber is surrounded by magnetic coils that create a magnetic field along the axis with a value of 0.004–1 T. The chamber is filled with working gas to a pressure of 0.001–1 Pa. At the ends of the chamber is a circular electrode or a system of annular electrodes, to which fixed electrical potentials ranging from 0.01 to 330 kV are applied during the experiment. The sign of the potential with respect to the ground potential can be different depending on whether a potential well or hill is created in the central part of the chamber. Plasma is initiated either by the application of voltage to the end

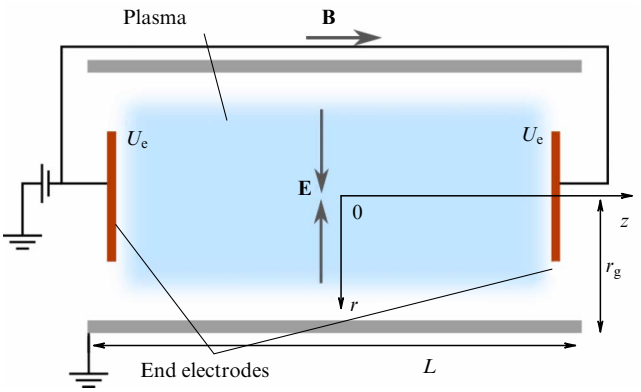

Figure 1. General setup of axisymmetric plasma systems with crossed $\mathbf{E} \times \mathbf{B}$ fields.

electrodes or using some additional source. Plasma electrons are usually magnetized, i.e., their free path greatly exceeds the Larmor radius. Plasma ions, depending on conditions, can be either magnetized or not.

The presence of a magnetic field in a plasma introduces anisotropy into the mobility of charged particles and, consequently, into their conductivity. Along magnetic lines, the mobility of the main current carriers, electrons, becomes significantly higher than that in the transverse direction. The limited current across the magnetic field leads to the accumulation of space charge on the system axis and the formation of an electric potential gradient. Thus, a radial electric field arises, also at some distance from the end electrodes. However, the electrode potential due to the cathode drop differs from the potential reproduced in the plasma volume.

In crossed electric and magnetic fields, charged particles are subject to drift in the $\mathbf{E} \times \mathbf{B}$ direction, and, if a radial electric field emerges, the plasma as a whole rotates in the azimuthal direction with a local angular velocity $\omega(r) = E(r)/rB$ [SI]. If $E(r)$ changes nonlinearly, an angular velocity gradient arises, which leads to Kelvin–Helmholtz instability and plays an important role in describing the instabilities of a rotating plasma [40].

From an experimental point of view, the direction of the radial electric field created in a rotating plasma is of importance. If the electric field is positive, i.e., the field is directed from the axis of symmetry, the end electrode is under a positive potential relative to the outer cylindrical surface. Vice versa, in the case of a negative radial electric field, i.e., the field is directed towards the axis, the central electrode is under a negative potential relative to the outer cylindrical surface. An important difference between these two cases is due to the ion current density usually being much less than the electronic one, while the area of the end electrodes in experimental setups is much less than that of the outer cylindrical surface. This implies that the discharge current between the electrodes when a negative potential is generated on the system axis can be noticeably less than in the case of a positive one.

3. Generation of a radial electric field in self-sustained discharges

We begin our consideration of experimental studies with systems in which plasma is created by maintaining a constant voltage on biased electrodes in the absence of additional ionization sources. The first review of such devices was published as early as 1971 [41]. Later, in the 21st century, reviews [22, 25] appeared. The scope of the last two reviews is not limited to self-sustained discharges. They cover a wide range of problems; however, the issue of potential distribution in the plasma volume is hardly addressed in these publications.

3.1 Penning discharge

The classic configuration of crossed $\mathbf{E} \times \mathbf{B}$ fields is a Penning discharge, also referred to as a reflex discharge [23]. A typical discharge circuit has the cylindrical symmetry displayed in Fig. 2.

The longitudinal magnetic field restricts the transport of electrons in the transverse direction. They oscillate between the cathodes and generate a large number of ionization events. Such a discharge can exist at fairly low pressures, down to 10^{-10} Pa [42]. Depending on gas pressure and the magnitude of the magnetic field, several modes are realized in the discharge that differ in the distribution of the plasma potential in the volume.

The first classification of modes was suggested in Ref. [43], where low-pressure Penning discharge modes were explored. Characteristics of the modes as functions of the magnitude of the axial magnetic field and gas pressure were obtained. The following biased electrodes were used: a cylindrical anode (internal diameter 2×10^{-2} m) made of stainless steel and two identical end flat molybdenum cathodes in the shape of a circle (distance between cathodes: 4×10^{-2} m). The anode potential varied from 250 to 4000 V. The cathodes were grounded. The magnetic field magnitude varied from 0.03 to 0.43 T. The plasma-forming gas was argon at a pressure from 4×10^{-6} to 10^{-2} Pa.

Figure 3 schematically displays the location of the discharge modes in coordinates B (magnetic field) and n (gas density) and the distribution of the electric potential in the chamber along the line connecting the cathode center and discharge chamber center, and then radially, the anode. The potential distribution in a vacuum is shown in Fig. 3c.

The absolute values of the mode boundaries vary over a wide range and strongly depend on the discharge geometry. At low pressure and weak magnetic fields, the discharge fails to ignite (Fig. 3b, region N). As the magnetic field increases at low pressures, the discharge gap breaks through, and a self-sustained discharge ignites. In this case, two modes are realized, depending on the magnetic field strength. In a weak magnetic field, the space charge is still small (region T), and the potential in the cell center is close to the anode potential V_a. As the magnetic field increases, a smooth

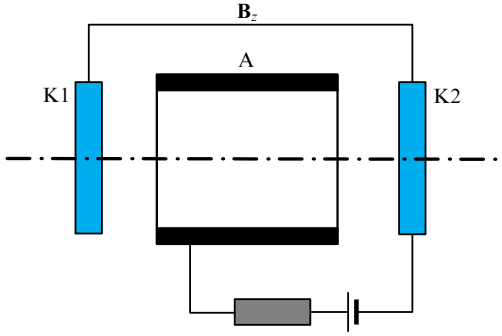

Figure 2. Reflex discharge scheme (A — anode, K1 and K2 — cathodes).

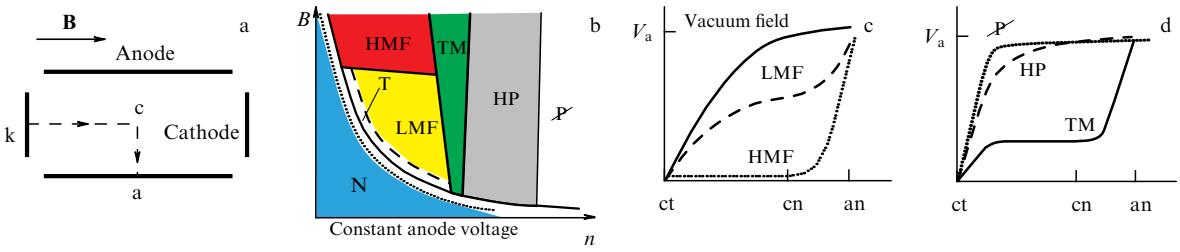

Figure 3. Direction of the measurement of potential in a Penning discharge (a); chart of Penning discharge modes (b); potential distribution (c, d) of plasma along the k → c → a (cathode → center → anode) path.

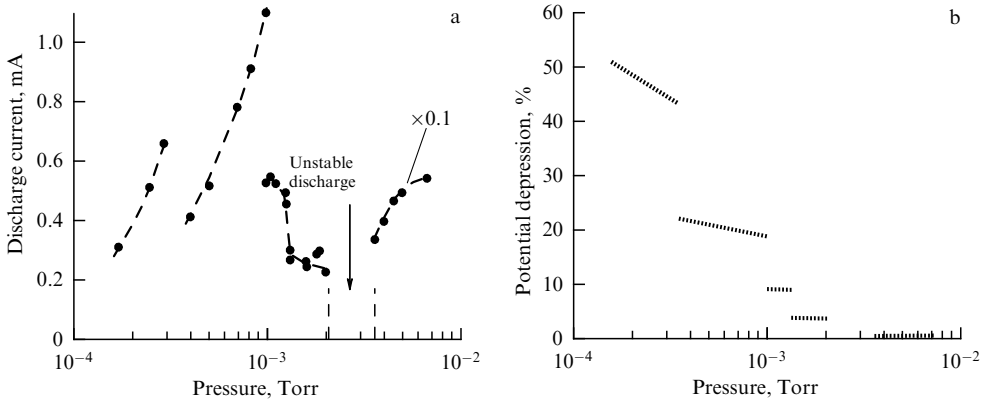

Figure 4. Dependence of discharge current (a) and potential drop (b) across the magnetic field on gas pressure at a constant voltage of 2 kV and magnetic field of 0.15 T [46].

transition occurs into the region called the Low Magnetic Field (LMF). The potential profile is greatly modified by a negative volume charge, which spreads over the entire volume of the discharge cell (Fig. 3c). This volume charge is formed by electrons, since their transport in the transverse direction is restricted. The ions that appear in the discharge move freely to the cathodes. With a further increase in the magnetic field, the potential on the axis drops to the cathode potential (Fig. 3c). In this mode, referred to as the High Magnetic Field (HMF), the entire potential drops in the radial direction, and there is no electric field along the axis. As the pressure increases, the discharge first transforms into an intermediate Transition Mode (TM) (Fig. 3d), and then into the High Pressure (HP) mode. In these modes, the discharge can exist only in the presence of a cathode potential drop; therefore, the potential on the axis approaches the anode potential with increasing pressure (Fig. 3d). The maximum value of the radial electric field is 200–300 kV m^{-1}.

Systematic experimental studies of the plasma potential on the discharge axis are reported in Refs [44–46], and theoretical studies are presented in Ref. [47]. In addition, the theoretical model developed in Ref. [36] was applied in Ref. [48] to the Penning discharge.

Reported in Ref. [46] are data from experiments with a Penning discharge, the geometry of which is described in Ref. [49]. In a pressure range from 10^{-2} to 1 Pa, five discharge modes were discovered, differing in current, which determine the pressure dependence of the potential in the discharge center. The plasma potential was determined based on analysis of the energy spectrum of ions using a high-resolution mass spectrometer [50].

To quantitatively describe the difference between the anode potential V_a and the potential at the discharge center V_0, the value of 'potential depression' is used, which presents the difference between these potentials as a percentage of the relative cathode-anode potential difference:

$$\Delta = \frac{V_a - V_0}{V_a - V_c} \times 100\% ,$$

where V_c is the cathode potential.

Figures 4 and 5 show the dependences of the 'potential depression' on the magnitude of the magnetic field, pressure, and discharge voltage for various modes. It can be seen in Fig. 4 that the 'potential depression' decreases with increasing pressure (at a constant discharge voltage of 2 kV and a magnetic field of 0.15 T). An important result is also the observation that a stable discharge was not obtained in a pressure range of 0.3–0.4 Pa.

Figures 5a, b clearly show that, in percentage terms, the reproduction of the cathode potential at the discharge center improves with increasing magnetic field (with a constant discharge voltage) and deteriorates with increasing discharge voltage (in a constant magnetic field). This is explained by the fact that an increase in the magnetic field hinders the transport of electrons in the direction transverse to the magnetic field, a factor that leads to an increase in the negative volume charge in the paraxial region. An increase in the discharge voltage leads to an enhancement of the electron flow to the chamber walls and a decrease in the volume charge.

Study [44] examined the potential on the discharge axis with a thermionic cathode as a function of the magnetic field and anode diameter. The plasma potential was measured using an emission probe. The discharge voltage was maintained at 280 V, the discharge current was 80 mA, and the hydrogen pressure was 0.665 Pa. Figure 6a shows the measurement results, which clearly show that, with increas-

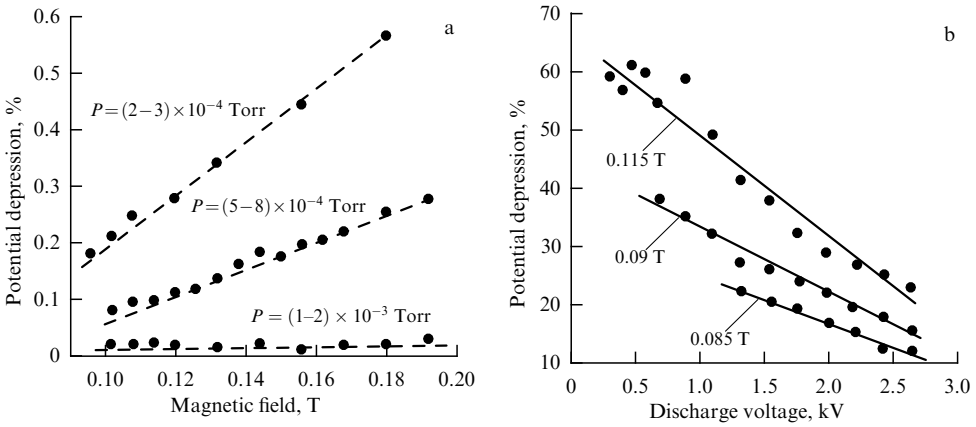

Figure 5. Dependence of potential drop across the magnetic field on pressure at a constant voltage of 1.75 kV (a) and on the discharge voltage in a constant magnetic field (b) [46].

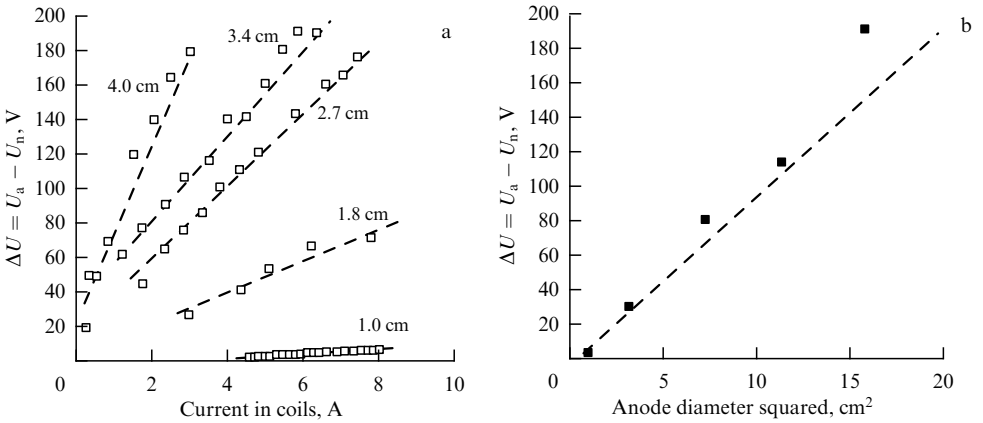

Figure 6. Dependence of the potential on the discharge axis on the magnetic field (a) and the anode diameter squared (in a magnetic field of 1.5 kG) (b) [44].

ing magnetic field (a current of 1 A corresponds to a magnetic field of 0.05 T), the plasma potential increases, but not equally for different values of the anode diameter. Figure 6b presents the dependence of the potential vs. the anode diameter for a magnetic field of 0.15 T.

In [45], the potential distribution in a Penning discharge in helium was studied. The experimental setup is shown in Fig. 7.

Distinct feature of these experiments is that, the diameter of the cathode was significantly smaller than that of the cylindrical anode, while in most other cases they are comparable. The experimental results not only complemented the understanding of the degree of influence on the plasma potential of factors such as the magnetic field strength, discharge voltage, and background gas pressure but also indicated the importance of the material and geometric parameters of the electrodes (shape and location).

Figure 8a presents the floating potential as a function of magnetic field [45]. The figure shows that an increase in the magnetic field leads not only to a change in the potential minimum but also to a contraction of the nonzero electric field region to the chamber center. Figure 8b shows the discharge current and floating potential V_p on the axis as a function of the discharge voltage. It can be seen that, by changing the voltage on the biased electrodes, the plasma potential can be increased, but only to a certain limit. It was shown in Ref. [45] that there is a limiting value, above which the plasma potential no longer responds to voltage changes.

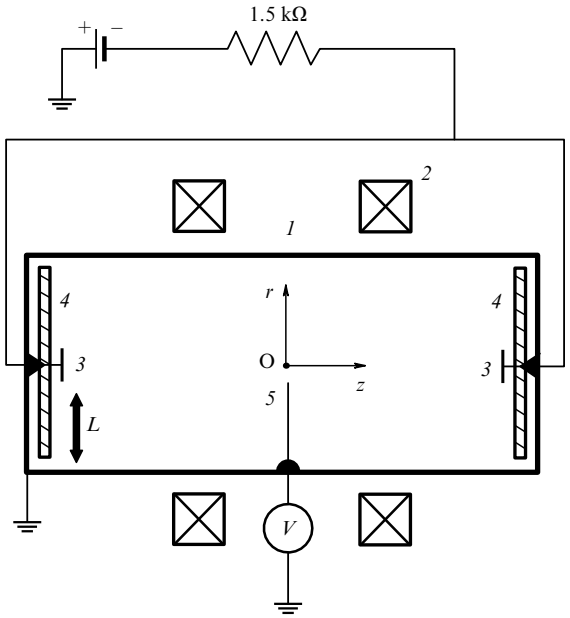

Figure 7. Experimental setup [45]. *1* — anode, *2* — Helmholtz coils, *3* — cathodes, *4* — dielectric plates, *5* — movable probe. *L* is the shortest distance between the anode and the cathode, and O is the center of the chamber. (Figure reproduced from [45] with permission from AIP Publishing.)

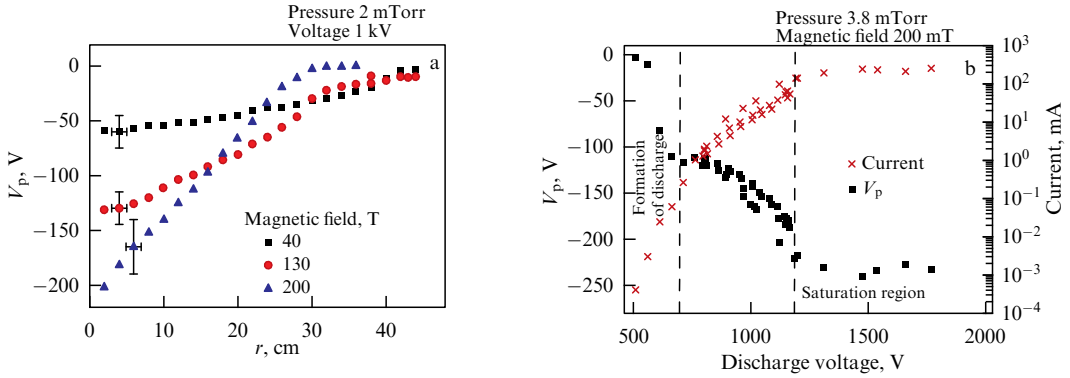

Figure 8. Floating potential in the Penning discharge in helium; radial profiles of floating potential in the chamber center for various magnetic field values (a), floating potential of plasma in the chamber center of and discharge current as functions of discharge voltage (b). (Figure reproduced from [45] with permission from AIP Publishing.)

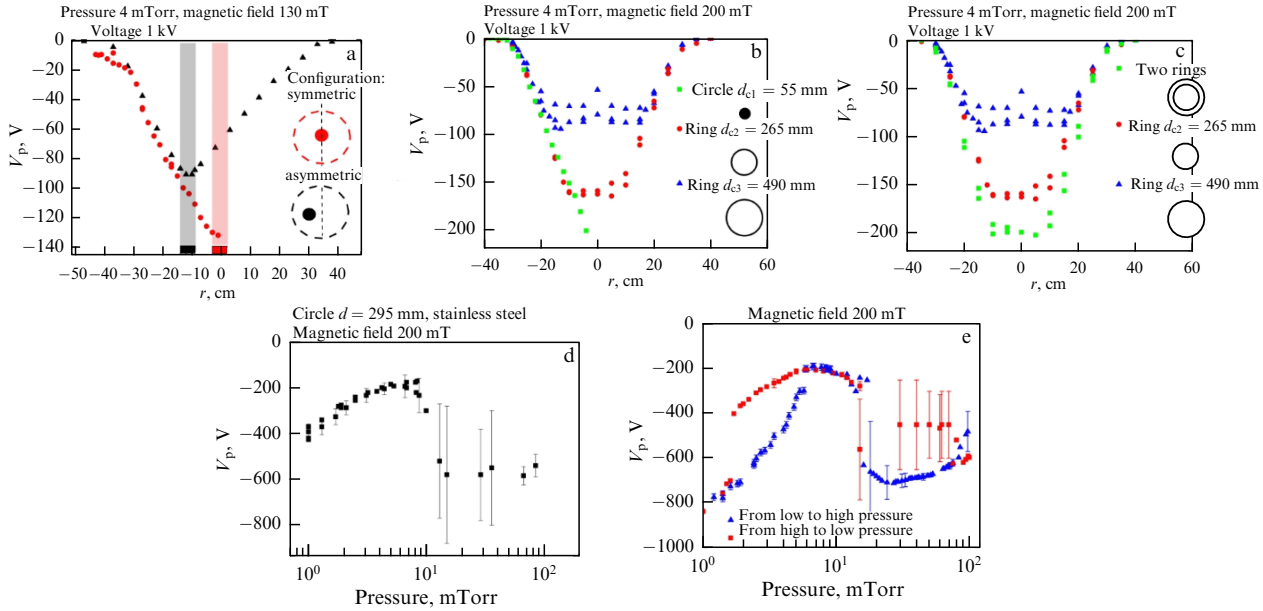

Figure 9. Influence of location (a), geometry (b, c), and material of the electrodes (d, e) on the potential in a plasma volume. (Figure reproduced from [45] with permission from AIP Publishing.)

With a further increase in voltage, only the cathode potential drop increases. A similar result is presented in Fig. 5b, if it is re-plotted for the absolute value of the plasma potential. The magnitude of the saturation potential depends on the magnetic field.

Another important factor affecting the potential distribution in a plasma volume with magnetized electrons is the geometry of the biased electrodes. Studies of this issue are also presented in Ref. [45], where an asymmetric configuration of electrodes (with the cathode shifted by 0.11 m from the symmetry axis of the cylindrical anode) and a configuration consisting of several concentric cathodes were considered. Radial distributions of potentials in the plasma volume for the indicated cases are presented in Fig. 9. The figure clearly shows that, in the case of a shifted cathode, the extremum of the potential also shifts. Along with this, the absolute value of the extremum decreases to the same value that existed at this coordinate in the axisymmetric case. The data presented indicate the key influence of the distance from the anode to the cathode in the direction transverse to the magnetic field on the value of the potential maximum. A similar situation occurs when such a distance is symmetrically changed using annular electrodes (Fig. 9b). The concurrent use of two nested annular electrodes, i.e., applying to them the same potential of 1 kV (pressure of 0.5 Pa, magnetic field of 0.21 T) leads to an increase in the plasma potential on the discharge axis compared to the potential acquired by the plasma when using only one of the electrodes (Fig. 9c).

Another important factor is the material of the electrodes. Figures 9d, e show the dependences of the plasma potential on the discharge axis as a function of gas pressure for biased electrodes made of stainless steel and aluminum, respectively. These figures clearly show that aluminum cathodes made it possible to obtain, under the same conditions, a higher absolute value of the potential in the plasma volume. In addition, hysteresis is observed when the gas pressure changes (Fig. 9e). The maximum value of the radial electric field is 0.5–1 kV m^{-1}.

3.2 Open traps based on self-sustained discharge

Studies conducted using open traps should be distinguished. They include both systems in which plasma is created exclusively due to end electrodes (self-sustained discharge) [51–55] and those where an additional ionization source is

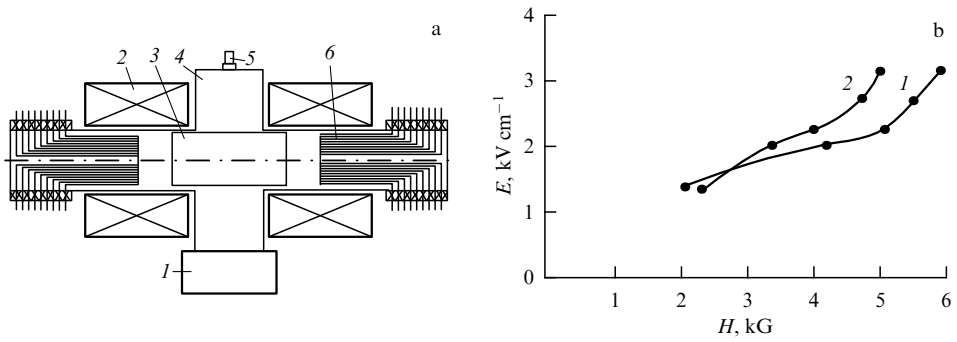

Figure 10. (a) PSP-1 setup: *1* — vacuum pump, *2* — magnetic field coils, *3* — liner, *4* — vacuum chamber, *5* — pulse valve, *6* — end electrodes. (b) Electric field strength as a function of magnetic field strength, below which plasma is stable, is *1* — 4×10^{-4} Pa, *2* — 2×10^{-3} Pa [55].

used [56–59]. In this section, we cover the first group. The second one is discussed later.

In essence, an open trap is nothing but a Penning discharge, but with a number of distinctive features. First, the discharges are pulsed. Second, the magnetic field is usually inhomogeneous and has a mirror geometry. Third, the voltages on the electrodes amount in such devices to tens of kilovolts. Fourth, located at the ends is not one electrode with a fixed potential, but a whole assembly of concentric electrodes, the potential on each of which can be maintained independently.

These studies were driven by the observation that the presence of a radial electric field in such a system could suppress flute instability and reduce radial losses of plasma [60]. The equation for flute oscillations in the presence of a radial electric field was derived by M Rosenbluth and A Simon [61], and the first experiments were carried out on the Ogra-1 apparatus (Kurchatov Institute of Atomic Energy, USSR) [62].

Paper [55] presents the PSP-1 apparatus (Institute of Nuclear Physics, Siberian Branch, USSR Academy of Sciences) (Fig. 10a). A voltage of 10–15 kV and a magnetic field of 0.5 T are applied to the end electrodes, gas (deuterium) is injected, and a Penning-type discharge is ignited. The characteristic electron density in the discharge is $n_e = 10^{15}$ m^{-3}; the electric field in the central plane is 30–100 kV m^{-1}; the discharge lifetime is about 5 ms; and the plasma rotation speed is about $(1-1.5) \times 10^5$ m s^{-1}.

The authors showed that at a fixed gas pressure a relationship exists between the electric field E at the end-electrode surface and the magnetic field B at which the discharge is stable. Figure 10b shows the dependence of E on B, where the plasma is stable below the indicated curves.

In the control experiment, the end electrodes were removed, and the potential to ignite the discharge was applied to a metal rod with a diameter of 1.5×10^{-2} m, located on the axis. In this case, the discharge was not stabilized.

Referring to [61], the authors argue that the distance between adjacent concentric end electrodes should be less than the Larmor radius of the ions so that they create a forced potential distribution in the plasma. In addition, it is noted that in these experiments the discharge stabilization effect is not affected by the type of radial potential distribution at the ends; however, the contact of the plasma with the conducting end faces turns out to be of importance (the importance of such contact was also noted in [63–65]).

Experiments on PSP-1 showed that the electric field in the central plane is much less than that which would

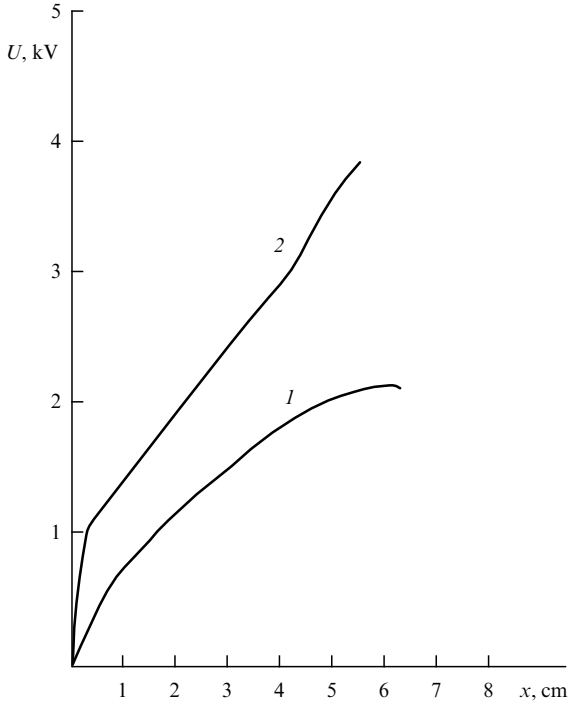

Figure 11. Radial profile of the plasma potential: *1* — without electron injection, *2* — with electron injection at a current of each injector of 1 mA. The x coordinate is measured from the chamber wall. End face voltage is 10 kV; magnetic field is 0.5 T; and pressure (deuterium) is 4×10^{-3} Pa [55].

correspond to the equipotentiality of the magnetic field lines. The contact of the plasma with the end cathodes turned out to be too weak to ensure a low cathode potential drop in the discharge. To improve this situation, injectors consisting of impregnated electrodes were installed. Figure 11 shows radial potential profiles measured in the central plane with and without additional electron injection. It can be seen from the figure that injection of electrons almost doubles the potential penetrating into the plasma. When the electron current from the injectors exceeded 10 mA, the discharge became unstable. The authors attribute this to an increase in the Larmor radius of the ions due to an increase in the plasma rotation speed.

Experiments using the PSM-1M equipment (Institute of Nuclear Physics, Siberian Branch, USSR Academy of Sciences) [54] (parameters are presented in Table 1, and the experimental setup is displayed in Fig. 12) showed that an increase in the plasma rotation speed, and therefore the

Table 1. Consolidated table of parameters of experiments on open traps based on self-sustained discharge.

Installation	Source	U_e, kV	U_{pl}, kV	E, kV m^{-1}	B, T	n_p, m^{-3}	p, Pa	T_e, eV	T_i, keV	t, ms	N	L, m D, m	Method of plasma potential measurement.
PSP-1	[55]	−10	1. −2 2. −3.8 (with thermal emission)	70	0.7(2)	10^{15}–10^{16}	H, D 0.004	—	0.1–0.2	5	10	$L = 0.6$ $D = 0.18$	Based on time of flight of SF_6^- [73].
PSM-1M	[54]	−20	—	300	0.5–1(2)	10^{19}	H 0.133	10	—	0–5	10	$L = 0.6$ $D = 0.2$	1. Analysis of broadening of spectral lines of optical radiation (Doppler shift). 2. Analysis of energies of charge-exchange neutral particles.
PSP-02	[71, 74]	−30	−7.5	500 (up to 1700)	0.6–0.8(3)	10^{17}–10^{19}	—	5	1.5–3	1–5	3	$L = 0.5$ $D = 0.12$–0.24	1. Floating probe. 2. Analysis of broadening of spectral lines of optical radiation (Doppler shift). 3. Analysis of energies of charge-exchange neutral particles.
PSP-2	[51]	−330	−265	1500	0.9–1.0(2.4)	4×10^{17}	H 0.013	5	45	0.5	24	$L = 1.6$ $D = 0.32$–0.51	Analysis of energies of charge-exchange neutral particles.
ISP	[72]	1. −1.4 2. −0.6	1. −1.4 2. −0.6	5–10	0.04–0.25	—	—	—	—	—	8	$L = 0.3$ $D = 0.28$	Analysis of energies of charge-exchange neutral particles.

Designations: U_e — maximum (in absolute value) potential at end electrodes; U_{pl} — maximum (in absolute value) plasma potential; E — electric field; B — magnetic field is indicated at center of the chamber on the axis. Mirror ratio is given in parentheses; n_p — plasma density; p — neutral gas pressure, T_e, T_i — temperature of electrons and ions; t — duration of experiment; N — number of electrodes at one end: number in parentheses indicates number of groups of electrodes that were under different potentials; L — distance between the ends; D — diameter of discharge cell.

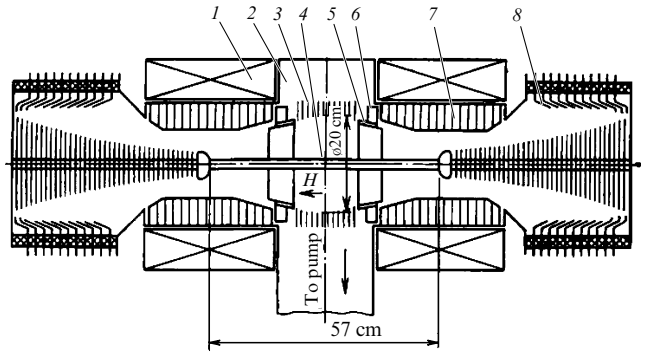

Figure 12. PSM-1M setup: *1* — magnetic field coils; *2* — vacuum chamber; *3* — liner; *4* — central electrode (tungsten); *5* — diaphragm (molybdenum); *6* — annular pulse valve; *7* — built-in magnetic discharge pump; *8* — protective rings of end insulators. $B = 0.5-1$ T [54].

electric field, can significantly interfere with gas release from the electrodes, which occurs under the effect of a flow of particles from the plasma. By degassing the electrodes (training in argon) and choosing the geometry and material of the electrodes, it was possible to obtain hydrogen plasma with a sufficiently high density (10^{19} m^{-3}) and rotation speed (5×10^5 m s^{-1}) in a quasi-stationary mode.

The central electrode (Fig. 12) with a radius of 3×10^{-2} m was maintained under a negative potential of 20–25 kV. The external electrode consisted of a set of grounded rings with an inner diameter of 0.2 m. A uniform potential difference was forcibly maintained on ten protective rings of the end insulators. The magnetic field B in the central region was 0.5–1 T. The radial electric field was 200 kV m^{-1}.

Papers [66–68] studied theoretical issues of stabilization of flute instability in the presence of radial electric fields and a longitudinal current. The main conclusion is that complete stabilization of (flute) magnetohydrodynamic (MHD) plasma instabilities in a centrifugal magnetic trap is possible by simultaneously using the effects of azimuthal 'slip' of plasma layers relative to each other (nonzero gradient of angular velocity) and introducing longitudinal electronic currents. Each of these effects separately results in a significant decrease in MHD activity in the plasma (reduction in the increment, contraction of the instability region in the parameter space), but the instability persists. It is only the simultaneous impact of both effects that provides complete MHD stabilization.

Optimal conditions for maintaining a self-sustained discharge correspond to $E/B = \text{const}$. In this case, slipping occurs due to the frequency of the azimuthal drift [60] being inversely proportional to the radial coordinate:

$$\omega = \frac{E}{Br} \sim \frac{1}{r} .$$

This value of radial slip is sufficient to suppress higher MHD modes of instability.

It was noted in [60] that the slip of layers can affect oscillations in both a stabilizing and destabilizing way. However, instabilities due to the action of this factor usually develop with special velocity profiles, for example, when they contain inflection points [69, 70].

Despite the success in stabilizing the discharge and increasing the plasma rotation speed obtained at the PSP-1 and PSM-1M facilities, the parameters achieved were not sufficient to implement thermonuclear fusion. An analysis in [52] showed that the design of a real reactor, which is based on an open trap with end electrodes, should include end electrodes with an electric field of the order of 10^4 kV m^{-1} and a total voltage drop of 5 MV.

As a result, the PSP-02 facilities (Institute of Nuclear Physics, Siberian Branch, USSR Academy of Sciences) [71] and PSP-2 (Institute of Nuclear Physics, Siberian Branch, Russian Academy of Sciences, Russia) [51] were created. A setup of the PSP-2 installation is shown in Fig. 13.

A radial electric field in the plasma was created by two identical systems of annular electrodes placed near magnetic mirrors. A potential could be independently applied to each pair of electrodes. The magnetic field in the central region was 0.9–1.0 T, and the maximum voltage at the electrodes was up to 500 kV. In a pulsed mode, hydrogen plasma with a density of 10^{18} m^{-3} was obtained; the plasma rotation speed turned out to be much higher than the critical value, $\sim 10^6$ m s^{-1}. The estimated average density of atomic hydrogen was 10^{18} m^{-3}.

The plasma potential and the potential of the electrodes in the central plane of the chamber, compared in Fig. 14, are in good agreement. The electric field in the central plane is about 1500 kV m^{-1}.

Study [72] reports the results of experiments on studying the distribution of electric fields at the ISP (Institute of Nuclear Physics, Siberian Branch, Russian Academy of Sciences, Russia) designed on the basis of a magnetic trap with axial magnetic and radial electric fields. The distribution of electric fields in the plasma was shown to coincide with the distribution specified at the end electrodes.

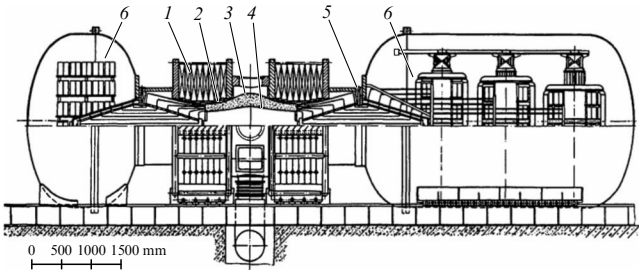

Figure 13. PSP-2 setup: *1* — magnetic field coils; *2* — plasma area; *3* — outer liner; *4* — inner liner; *5* — electrode system; *6* — high-voltage unit.

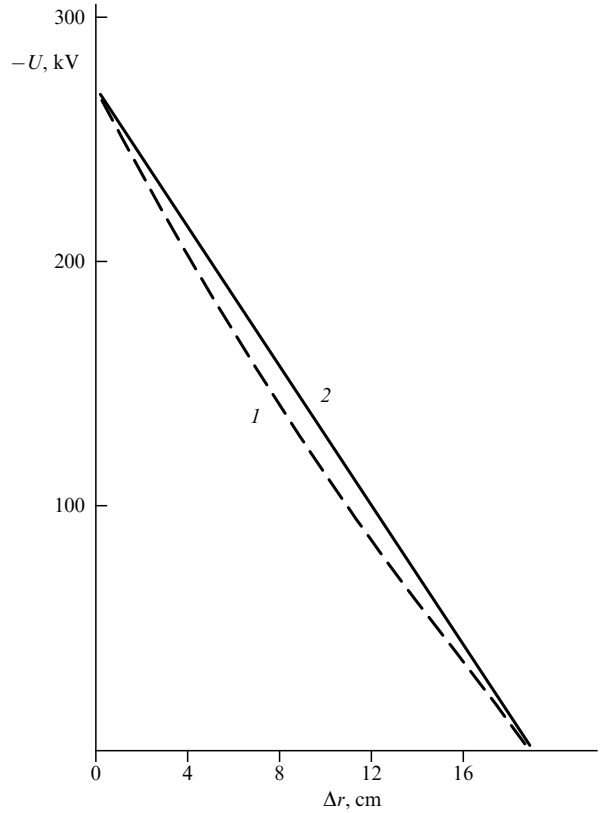

Figure 14. Distribution of potential in central plane $U(r)$ (*1*) and potential applied to end electrodes (*2*) [51].

4. Generation of a radial electric field by end electrodes in the presence of an additional ionization source

Considered in the previous section were systems in which the end electrodes were concurrently creating a radial electric field and maintaining the discharge. This configuration limits the ability to control the potential profile, since, in this case, attempts to change the potential on the biased electrodes or their geometry significantly affect the characteristics of the discharge itself, and not just the potential profile in the plasma. In this section, we consider facilities in which the potential in the plasma volume is created by electrode system independent of the plasma generation system.

Below, all experiments are divided based on the purpose of the research. This is of importance since the research goal determines the parameters of the experiment. For example, for nuclear fusion and plasma mass separation problems, an electric potential of several hundred volts is maintained on the electrodes, while, in studying instabilities and some other properties of plasma, only a few ten volts are usually applied to the electrodes.

4.1 Influence of angular velocity gradient on plasma instabilities

4.1.1 Q-machines. Some of the first attempts to create a radial electric field in a magnetized plasma column in a nonself-sustaining discharge were realized using Q-machines, where plasma is created due to the contact ionization of gas on a heated plate located at one or both ends of a cylindrical chamber [75, 76] (Fig. 15). The gas ionization potential should be less than the work function of electrons escaping from the

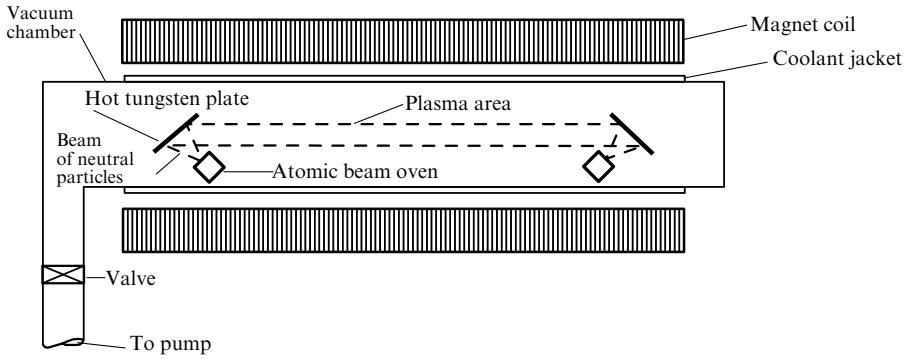

Figure 15. Schematic of the Q-machine. (Figure reproduced from [76] with permission from AIP Publishing.)

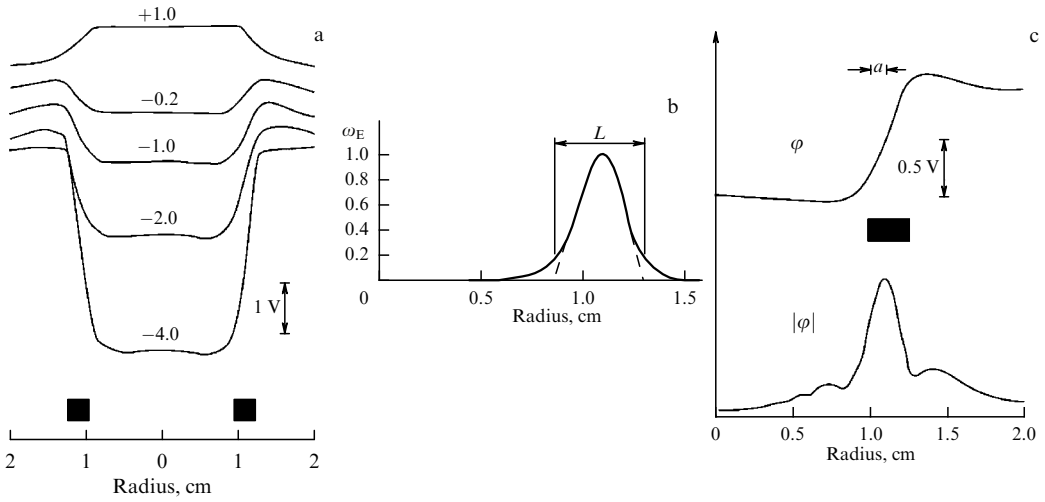

Figure 16. (a) Radial profile of the floating potential for a segmented end electrode at $B = 0.32$ T and $n = 4 \times 10^{15}$ m^{-3}. Black squares represent size of the gap between concentric electrodes. Number next to each curve indicates voltage (in volts) between inner and outer electrodes, (b) Radial distribution of angular frequency of plasma rotation in $\mathbf{E} \times \mathbf{B}$. Shear velocity layer is slightly wider than gap width (0.24×10^{-2} m). (c) Radial profile of potential φ and amplitude of fluctuations of floating potential $|\varphi|$ at a potential on the electrodes of 1 V, $n = 2 \times 10^{16}$ m^{-3}, $B = 0.38$ T, and a is the Larmor radius of ions. (Figure reproduced from [81] with permission from AIP Publishing.)

hot plate; therefore metal vapors are usually used. The hot plate also emits electrons to ensure quasi-neutrality of the plasma. A thin sheath is formed near the electrode, the properties of which are determined by the balance between the flows of electrons and ions from the surface. Located outside this sheath is a quasi-neutral plasma, which is kept from flying away in the radial direction by the magnetic field. Such plasma is more stable than that created in a self-sustained discharge. However, at the column periphery, oscillations, so-called 'edge oscillations,' persist, first observed in [77]. It was shown in [78, 79] that the main mechanism of these oscillations is associated with shear flow during azimuthal rotation.

As already noted in Section 3.2, a cylindrical plasma column placed in a uniform magnetic field B and a radial electric field $E(r)$ rotates relative to the axis with a local angular velocity $\omega(r) = E(r)/rB$. If $E(r)$ changes nonlinearly with the distance r from the axis, the plasma rotates in a nonuniform way, which can lead to the emergence of an angular velocity gradient.

In [80, 81], the influence of the transverse gradient of angular velocity on fluctuations of the potassium plasma potential was studied. The length of the plasma column was 1.1 m and its diameter was 4.4×10^{-2} m. The potential of the cold plate was less than that of the hot plate. An inhomogeneous radial electric field was created using segmented concentric electrodes. To do this, a system of biased electrodes was installed at the end, which most often consisted of two parts: a round inner electrode and an annular outer electrode. The electrodes were separated by an insulator. A potential difference was applied between the electrodes. The size of the inhomogeneity region was several Larmor radii of the ions.

A typical radial profile of the equilibrium floating potential is shown in Fig. 16a [81], which shows that the potential difference between the electrodes (the number next to each curve) corresponds fairly well to the measured drop in plasma potential. The electric field varied from 0 to 1850 V m^{-1}.

Figure 16b shows the radial dependence of the angular velocity $\mathbf{E} \times \mathbf{B}$ of the drift (plasma rotation frequency). It can be seen that the dimensions of the electric field region (approximately 0.45×10^{-2} m) are larger than the gap between the electrodes (0.24×10^{-2} m). Figure 16c presents the radial dependences of the plasma potential and the amplitude of fluctuations of the floating plasma potential. The localization of the maximum amplitude of fluctuations coincides with the region of the inhomogeneous electric field. The authors of the study conclude that the observed fluctuations are due the transverse Kelvin–Helmholtz instability. In electric fields less than 850 V m^{-1}, low-frequency fluctuations (< 50 kHz) were observed. In strong-

er fields, low-frequency oscillations were suppressed, but at the same time, fluctuations emerged with a frequency higher than the ion-cyclotron frequency.

Further studies [82] with segmented electrodes on Q-machines showed that, in addition to long-wave (wavelength greater than the characteristic size of the region with an angular velocity gradient) and low-frequency oscillations (frequency much lower than the ion cyclotron frequency) associated with the Kelvin–Helmholtz instability, an electric field transverse to the magnetic field can be the reason for the emergence of short-wave oscillations similar to the Kelvin–Helmholtz instability due, however, to inhomogeneous-energy-density driven (IEDD) instability [83]. In addition, the longitudinal current to the electrodes generates current-driven electrostatic ion-cyclotron (CDEIC) instability and universal drift potential relaxation instability (PRI) [84]. In general, for a combination of a transverse electric field and a longitudinal electric current, these instabilities build up much faster than when each of the two specified free energy sources operates separately [83].

In [85, 86], end concentric electrodes were used to create a radial electric field (relative to the direction of the magnetic field) and longitudinal current.

The characteristic parameters of the experiments were as follows: radius of the potassium plasma column: 3×10^{-2} m, length: 0.8 m, density: $n \approx 10^{15}$ m^{-3}, magnetic field: $B = 0.15$ T, and pressure of neutral particles: 4×10^{-4} Pa.

The radial profile of the plasma potential in a plane 2×10^{-2} m away from the electrode was determined using a emissive probe for various combinations of bias potentials between the inner circular electrode and the outer annular electrode. Figure 17 shows that the potential difference between the annular electrode $V_a = 11$ V and the circular electrode $V_b = -3 - 18$ V does not correspond to the potential difference in the plasma. In addition, the authors point out that the radial electric field in the plasma increases with increasing potential difference between electrodes of up to 25 V (the gap between the electrodes is 1×10^{-3} m) reaches a value on the order of 300 V m^{-1}. However, if the potential difference increases further, the electric field 'saturates' and varies only slightly. This statement is fairly important, since it may imply the existence of fundamental limitations on the ability to vary the plasma potential using end electrodes.

All in all, a lot of experiments with segmented electrodes were carried out on Q-machines. The plasma potential differed significantly from the potentials of the end electrodes. The potential variation in the plasma usually did not exceed 10 V.

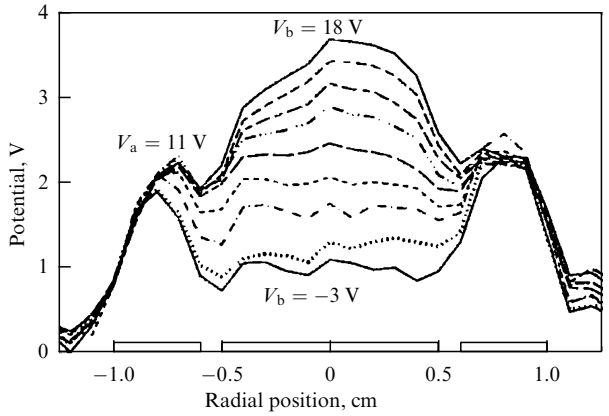

Figure 17. Radial profile of plasma potential in the Q-machine. (Figure reproduced from [85] with permission from AIP Publishing.)

4.1.2 Radial electric field in a plasma generated by gas discharge. The influence of the angular velocity gradient on the buildup of plasma instabilities and fluctuations of the electric potential was studied in systems where the plasma was generated by a gas discharge. At the SPSC installation (Space Physics Simulation Chamber, Naval Research Laboratory, USA) [87, 88], an argon plasma was created by a microwave discharge in a vacuum chamber with a diameter of 1.8 m and a length of 5 m. The installation setup is displayed in Fig. 18.

Discharge parameters are: diameter and length of the plasma column is 0.5 and 2 m, respectively; plasma density is 3.5×10^{13} m^{-3}; magnetic field is 4 mT; and density of neutral particles is 6×10^{17} m^{-3}. To create a radial electric field, an electrode was used, which consisted of 11 concentric coplanar conducting rings. The smallest and largest radii were 0.1 and 0.3 m, respectively. Applying different potentials to different rings made it possible to alter the potential profile and, as a result, create a localized electric field.

Figure 19 shows the radial dependences of the plasma potential and the electric field at a distance of 0.145 m from the electrode when 7 outer rings were at a potential of +20 V relative to the grounded chamber, while the potential of the other rings was −10 V. To determine the potential, a emission probe was used. It can be seen that the electric field is localized in the annular region $0.04 < r < 0.11$ m with a maximum of about 60 V m^{-1} [88] (Fig. 19). It should be noted that, at significant distances from the electrode (up to 0.88 m), the radial profile of the field changed only slightly. The magnitude of the electric field was primarily determined by the potential of the outer rings.

In the mode with a low longitudinal current (below the threshold for excitation of CDEIC instabilities), the radial electric field was shown to generate broadband $\delta f/f \approx 30\%$ fluctuations in the plasma density at the level of $\delta n/n \approx 15\%$. Such fluctuations can be associated with IEDD waves. The threshold for the occurrence of fluctuations is at the level of 40 V m^{-1}. The frequency of these fluctuations, depending on the ratio of the drift velocity in crossed fields to the thermal velocity of the ions, varies in the range of $(1.5 - 2.6) f_{ci}$, where f_{ci} is the ion cyclotron frequency. This frequency shift is due to the Doppler shift.

The HelCat installation (Helicon-Cathode, University of New Mexico, USA) (Fig. 20) was designed to study a wide class of phenomena in plasma (instabilities, transport, etc.). Plasma can be produced in this facility using two sources — a helicon source and a thermionic cathode — located at

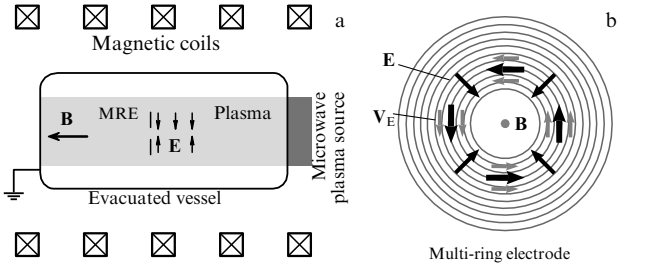

Figure 18. Setup of experimental SPSC installation (a) and end electrode (b). (Figure reproduced from [88]. Copyright (2023) by the American Physical Society.)

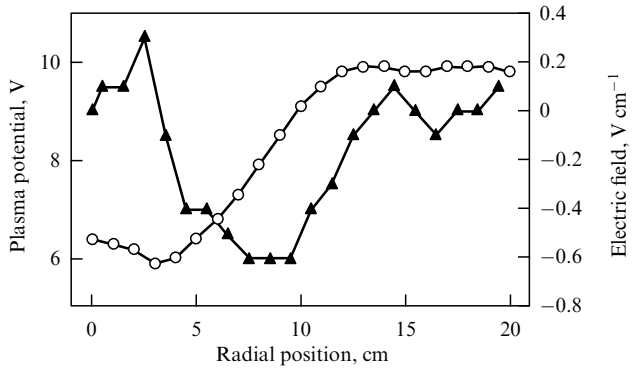

Figure 19. Radial profiles of plasma potential (circles) and electric field (triangles). Four internal electrodes $r < 8$ cm are at a potential of -10 V and seven external electrodes $r > 10$ cm are at a potential of $+20$ V. (Figure reproduced from [88]. Copyright (2023) by the American Physical Society.)

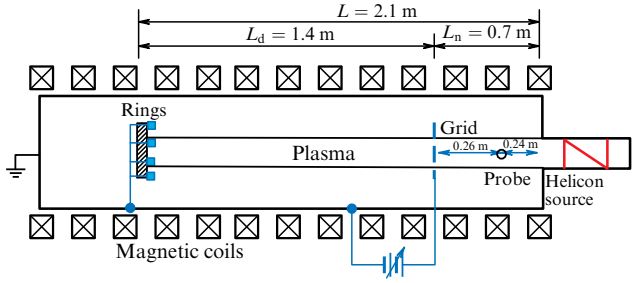

Figure 20. HelCat setup. (Figure reproduced from [91] with permission from AIP Publishing.)

opposite ends of a four-meter vacuum chamber. Magnetic coils can provide an axial magnetic field of up to 0.22 T. Helium and argon were used as plasma-forming gases. Peak densities in a plasma column 0.13 m in diameter were $10^{16} - 10^{20}$ m^{-3} [89, 90].

In addition to the end electrodes consisting of concentric rings located at the opposite end from the plasma source, the HelCat also used on the plasma source side a 50–70% transparent metal grid, to which a potential was also applied.

Figure 21 shows the radial dependences of the electric field for various bias potentials of the annular electrodes. Studies have shown that the use of a negative bias on the electrodes does not lead to a decrease in the plasma potential but significantly enhances the amplitude of broadband fluctuations in the plasma density (Fig. 22a). Estimates made in Ref. [36] showed that, at the selected pressure (0.33 Pa) and a magnetic field of 35–44 mT, a negative potential on the axis of such a system cannot be created. However, an increase in the magnetic field leads to an increase in the amplitude of fluctuations (Fig. 22b) [91]. A small positive bias of the end electrode potential on the order of $(3-7)T_e$ leads to suppression of oscillations. A higher positive bias potential $(10-15)T_e$ leads to an increase in the level of fluctuations and, apparently, to an buildup of the PRI instability [92].

There is some uncertainty in interpreting the spatial distribution of potential in HelCat experiments. Earlier papers reported data obtained using a floating probe taking into account the electron temperature, which indicated the presence of a radial electric field [93, 94], while in later studies a flat plasma potential profile was obtained [92]. This ambiguity may be due to challenges in interpreting data

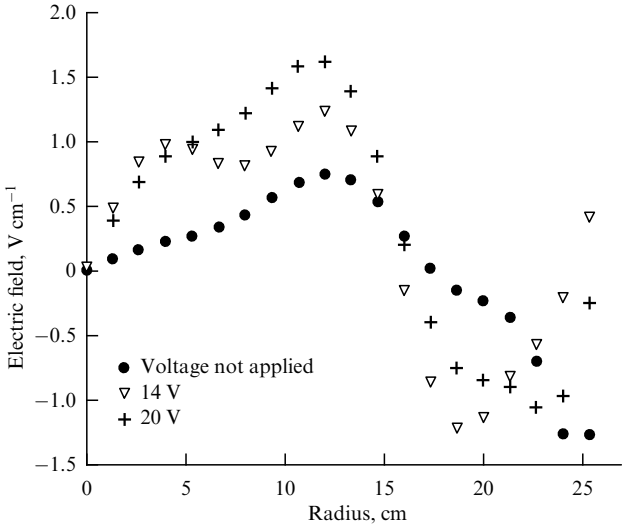

Figure 21. Radial dependences of electric field for various bias potentials of ring electrodes in the HclCat installation. Argon, $B = 35$ mT; neutral particle pressure 0.32 Pa; discharge power 1.6 kW [90].

from a floating probe. In some cases (for example, in an RF discharge), the difference between the floating potential and the plasma potential can differ significantly from the value of $5.2\,T_e$ (for argon) due to the nonMaxwellian function of electron velocity distribution [95].

The problems of plasma instabilities and their impact on particle transport are addressed in studies [96–99], performed at the LAPD facility (Large Plasma Device, University of California, Los Angeles, USA). The installation setup is displayed in Fig. 23a. Located in a vacuum chamber 18 m in length and 1 m in diameter were a barium-oxide thermal cathode with a diameter of 0.73 m and a molybdenum-grid anode at a distance of 0.5 m from the cathode. Typical discharge parameters were $n_e \leqslant 5 \times 10^{18}$ m^{-3}, $B < 0.2$ T, and the plasma-forming gas was helium. When a potential difference of 40–60 V is applied between the cathode and the anode, the electrons of the hot cathode are accelerated and ionize the gas, including in the main chamber behind the anode grid. The shape of the radial profile of the floating potential is displayed in Fig. 23b. In the main volume, the side section is maintained under positive potential. This leads to the formation of a negative electric field on the order of 300 V m^{-1} at the periphery of the column (the potential on the system axis is more negative). It was shown in [97–99] that, when the negative bias increases to 100 V, transverse transport switches from the Bohmian regime to the classical one.

Studies were also carried out in the plasma decay mode [100]. After the main barium cathode is deactivated, the electron temperature drops to 0.2 eV in approximately 2 ms. The plasma density also begins to decrease, but approximately an order of magnitude more slowly: from 10^{18} to 10^{17} m^{-3} in 10 ms. On the opposite side of the installation there is an electrode with a negative bias. It has been shown that a radial electric field can only be created if electrons are injected from this cathode. Without injection, the plasma potential does not respond to the electrode potential.

Attempts to enhance the influence of electrodes on the radial potential profile using a thermal cathode were also made in [101]. Argon plasma, created by an RF induction discharge, entered a cylindrical region 0.8 m in length and

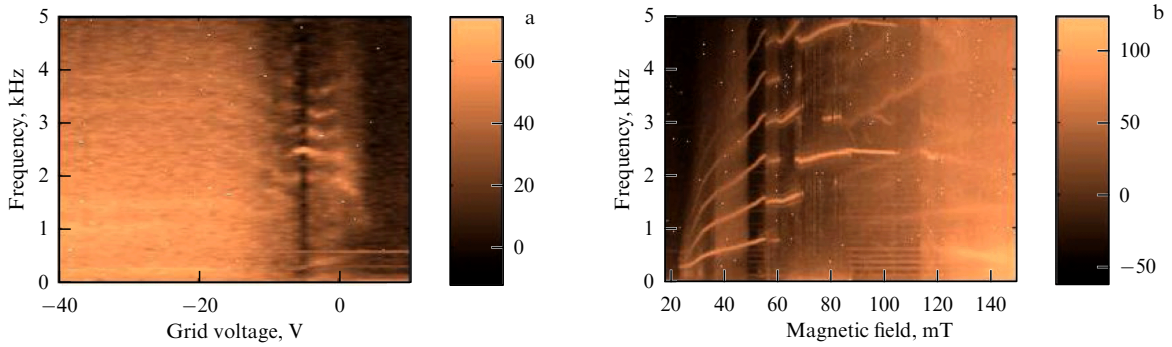

Figure 22. Spectrograms of oscillations of ion saturation current to the Langmuir probe in the HelCat installation as a function of bias potential of grid electrode (a) at 35 mT and the magnetic field (b). (Figure reproduced from [91] with permission from AIP Publishing.)

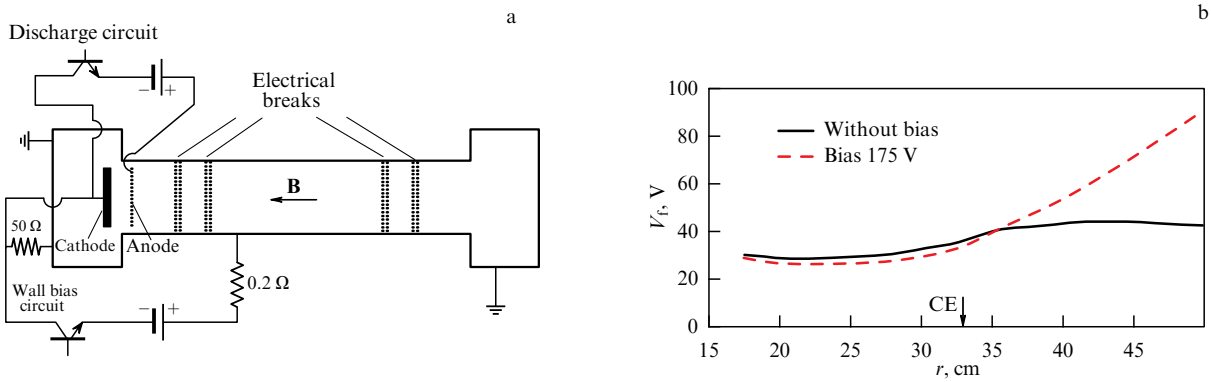

Figure 23. (a) LAPD setup, (b) radial profile of floating potential, CE is cathode boundary. (Figure reproduced from [97] with permission from AIP Publishing.)

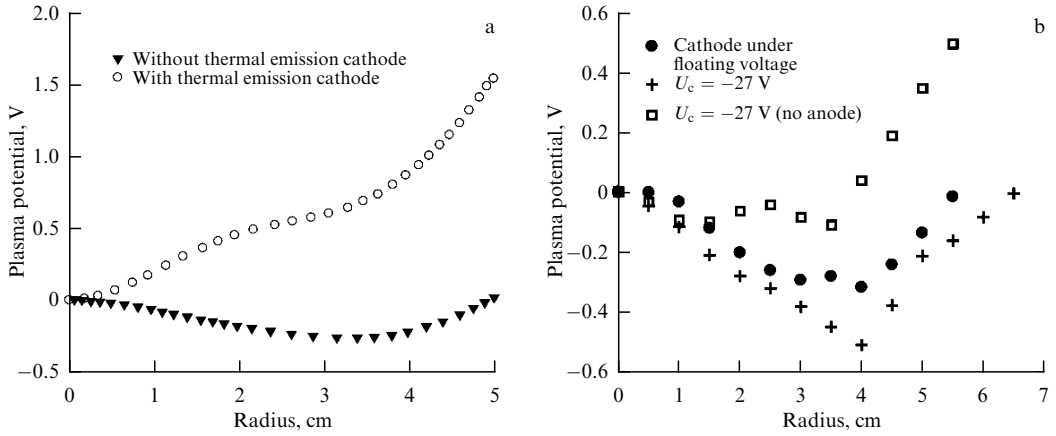

Figure 24. Plasma potential profile for one cathode (cathode potential −40 V) (a); plasma potential profile for two cathodes (b) at the installation [101].

0.2 m in diameter with grounded walls. Two configurations of emission electrodes were used. In the first one, the thermal cathode was located on the discharge axis, while, in the second configuration, two thermal cathodes were located on the periphery of the column, and the anode was located on the discharge axis. Typical discharge parameters were: argon pressure, several tenths of Pa, $n_e \approx 10^{18}$ m^{-3}, $B \leqslant 0.15$ T. Figure 24 shows the plasma potential profiles for one cathode (Fig. 24a) and two cathodes (Fig. 24b) [101].

A similar experiment [102] with the parameters of an RF discharge in argon — pressure 0.133 Pa, magnetic field 0.02 T, plasma column diameter 0.1 m — successfully demonstrated a noticeable influence of the cathode temperature on the radial profile of the floating potential of the plasma (Fig. 25). The largest potential gradient was approximately 150 V m^{-1}.

Table 2 presents consolidated parameters of experiments on installations with an additional ionization source and with a biased potential of the end electrodes.

4.2 Open ion traps with an additional ionization source

Studies [103–106] showed that, due to the presence of an electric field at the plasma column periphery, transverse losses in thermonuclear fusion installations can be reduced. This observation stimulated studying the feasibility of

Table 2. Consolidated table of parameters of experiments with an additional ionization source and potential bias of end electrodes.

Installation	Source	U_e, V	U_{pl}, V	E, V m^{-1}	B, mT	n_p, m^{-3}	p, Pa	T_e, eV	T_i, eV	t, s	N	L, m D, m	Plasma creation method	Method of plasma potential measurement
Q-3 machine	[81]	1. −4 2. +1	1. −4 2. +1	1850	320	4×10^{15} (up to 2×10^{16})	K	0.18	—	Cont.	2	$L = 1.1$ $D = 0.04$	Surface ionization	Floating probe
Frascati Q-machine	[80, 115]	1. −1 2. +1	1. −1 2. +1	100	300	6×10^{16}	Cs, K	0.2	0.2	Cont.	2	$L = 0.9$ $D = 0.08$	Surface ionization	Floating probe
West Virginia Q-machine	[86]	19	1	−380	150	10^{15}	K	0.2	0.2	—	2	$L = 0.8$ $D = 0.02$	Surface ionization $T = 2000$ K	Emissive probe
Improved Q-1 machine	[116, 117]	+300	+3.9	—	210	10^{16}	K	—	—	—	2	$L = 0.92$ $D = 0.05$	Surface ionization $T = 2000$ K	Emissive probe
SPSC	[87, 88]	−30	−14	60	4	4×10^{13}	Ar 0.53×10^{-2}	1	0.05	Cont.	11(2)	$L = 2$ $D = 0.3$	Microwave discharge $P = 0.17$ kW	Emissive probe
HelCat	[89–94]	+20	+20	100	35	$10^{18} - 10^{19}$	Ar 0.32	1–5	—	0.25	6(1)	$L = 2.6$ $D = 0.13$	RF discharge $P = 1.6$ kW $f = 10$ MHz	Floating probe
LAPD	[96–99]	−220 thermionic cathode	−200	700	40	3×10^{18}	He 0.013	6–8	1	$4 \times \times 10^{-3}$	1	$L = 17.6$ $D = 0.6$	Electron beam 40–60 V	Triple probe
Univ Lyon machine	[101, 102]	−60 thermionic cathode	−14	150	20	5×10^{18}	Ar 0.132	3	0.3	1	1	$L = 0.8$ $D = 0.2$	RF discharge $P = 1-3$ kW $f = 13.56$ MHz	Emissive probe

Designations: U_e — maximum (in absolute value) potential at end electrodes; U_{pl} — maximum (in absolute value) plasma potential; E — electric field; B — magnetic field is indicated at center of the chamber on the axis; n_p — plasma density; p — neutral gas pressure, T_e, T_i — temperature of electrons and ions; t — duration of experiment; N — number of electrodes at one end; figure in parentheses indicates number of groups of electrodes that were under different potentials; L — distance between ends and D — diameter of discharge cell. Q-3 machine — Plasma Physics Laboratory, Princeton University, USA; Frascati Q machine — Laboratori Gas Ionizzati, Assiciazione Euratom-CNEN, Frascati, Rome, Italy; West Virginia Q machine — West Virginia University, USA; Improved Q-1 machine — Department of Physics, University of California, USA; Univ Lyon machine — University of Lyon, France.

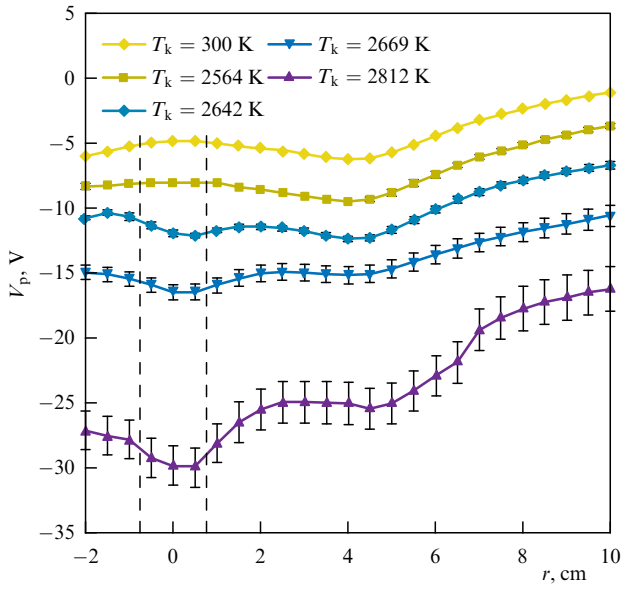

Figure 25. Plasma potential profile at various cathode temperatures under a magnetic field of 0.02 T and pressure of 0.133 Pa (Ar); cathode potential −60 V [102].

creating a radial electric field in open traps. Here, as in Section 3.2, in the context of stabilization of MHD instabilities, plasma contact (line-tying) with conducting walls is of importance [63, 107, 108].

The first experiments were carried out using ambipolar traps (tandem mirrors) [109, 110] proposed in [111, 112]. In such a trap, the plasma is confined from escaping through the ends using electrical ambipolar barriers created in double magnetic mirrors at the solenoid ends. In other words, at each end of the solenoid, an additional mirror cell is installed, inside which plasma of a certain density is maintained.

Attempts to control the plasma potential using end electrodes were made using the Phaedrus Tandem Mirror setup (University of Wisconsin, USA) [57, 113, 114]. Hydrogen plasma was created by RF heating; its density and magnetic field were 2×10^{18} m^{-3} and 60 mT (in the central part), and 7×10^{18} m^{-3} and 0.27 T (at the ends). Control of the radial potential profile was assumed to be a key element for the entire experimental program of this installation, since, after the longitudinal losses of particles were reduced, it was the transverse losses that became the main channel of losses, and the radial electric field could exert a decisive effect on them.

Figure 26a presents a setup of four electrodes located at each end of the apparatus. The bias voltage was applied to the third electrode (middle), while the remaining electrodes were

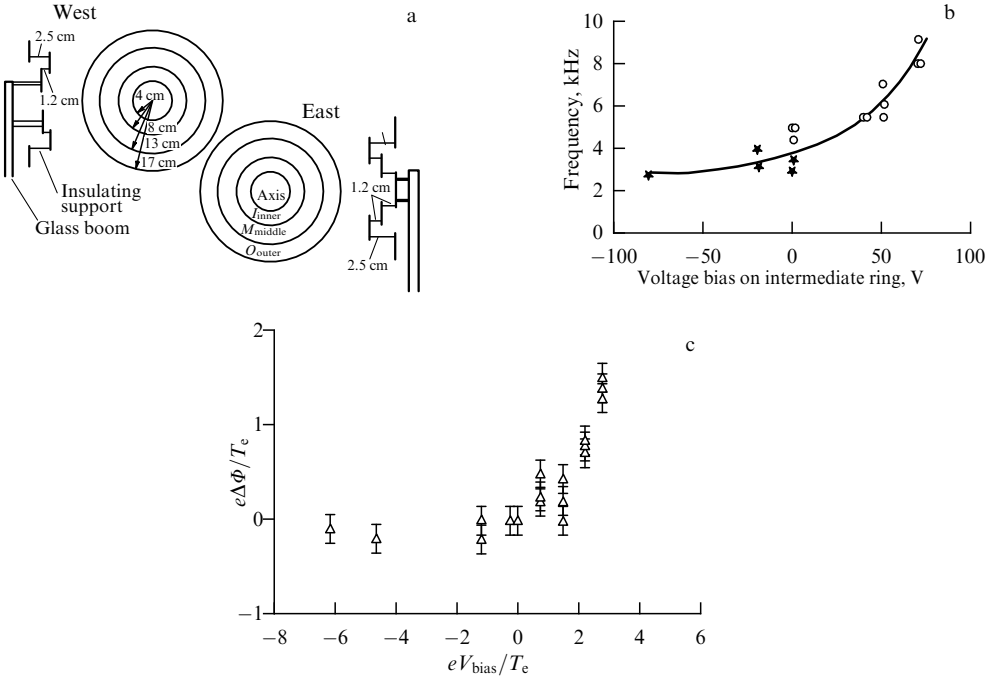

Figure 26. (a) Setup of end electrodes of Phaedrus Tandem Mirror installation; (b) dependence of fluctuation frequency on bias potential of end electrodes [57]; (c) dependence of plasma potential on bias potential, normalized to electron temperature of 15–20 eV. (Figure reproduced from [113] with permission from AIP Publishing.)

grounded. With increasing bias, the frequency of floating potential oscillations increased (Fig. 26b), which is associated with a corresponding increase in the frequency $\mathbf{E} \times \mathbf{B}$ of plasma rotation. In the experiments, the plasma potential could only be affected by a positive bias (Fig. 26c). The maximum electric field was approximately 1 kV m^{-1}. If the bias was negative, the plasma potential did not change.

At a bias potential of more than 60–70 V, the formation of plasma became unstable and could not be supported by RF heating. In the control experiment, the electrodes at one of the ends were replaced with a thermionic ring, which was under a floating potential. An increase in the heating power of the ring, and consequently the thermionic current, led to an enhanced plasma stability, which is consistent with the concept of plasma stabilization due to good contact with the conducting ends [108].

Another important result obtained at this installation is the measured time of response of the plasma potential and the axial loss current to the application of potential to the end electrodes, which was less than 50 μs.

Another ambipolar trap, Gamma 10 (Plasma Research Center, University of Tsukuba, Japan) [118], also used end electrodes to control the radial electric field [58, 119]. The plasma density in the central part was 10^{18} cm^{-3}, the effective diameter was 0.25 m, and the magnetic field was 0.8 T. Data on the potential Φ_C and the strength E_r of the radial electric field in the central region vs. the bias potential V_B supplied to the electrodes are presented in Table. 3. At zero bias, the potential in the central chamber was on the order of 1.5 kV, and decreased with a negative bias. Although the plasma potential can be controlled in such a system using the bias potential of the end electrodes, including in the negative bias region, it turns out that the solution optimal for plasma confinement is not to use a bias on the end electrodes at all.

Table 3. Data on potential Φ_C and intensity E_r of radial electric field in central region of Gamma 10 installation as a function of bias potential V_B applied to electrodes.

V_B, V	Φ_C, V	E_r, kV m^{-1}
750	2200 ± 150	17.6 ± 1.2
0	1600 ± 150	11.5 ± 1.1
−500	1000 ± 100	7.9 ± 0.8
−1000	600 ± 100	4.6 ± 0.8
−1500	100 ± 50	0.6 ± 0.3
−2000	-200 ± 50	-1.8 ± 0.4

The KMAX installation (Keda Mirror with AXisymmetricity, University of Science and Technology of China, China) [59] was used to study the effect of the end electrode on the potential of the target (starting) plasma (Fig. 27a). The target plasma, which was created by a helicon source with a power of 1.5–2 kW, was injected from the end opposite the potential-setting electrodes. In this experiment, the bias voltage was applied only to the central disk-shaped electrode, while the annular electrode was maintained at a floating potential. Figures 27a, b show the radial and axial profiles of the floating potential at various biases of the end electrode. The influence of the bias potential on the plasma potential is small; almost the entire voltage (330 out of 350 V) drops in the near-electrode sheath.

At the GDT (gas-dynamic trap) installation (Budker Institute of Nuclear Physics, Siberian Branch, Russian Academy of Sciences, Russia) [56, 120], the concept of vortex plasma confinement was implemented [121]. Four concentric biased electrodes were located behind the magnetic mirrors of the central solenoid. The central electrode was grounded, while a positive bias from 0 to +300 V was applied to other electrodes. Thus, the electric field was directed towards the system axis. The plasma comprised two components. The

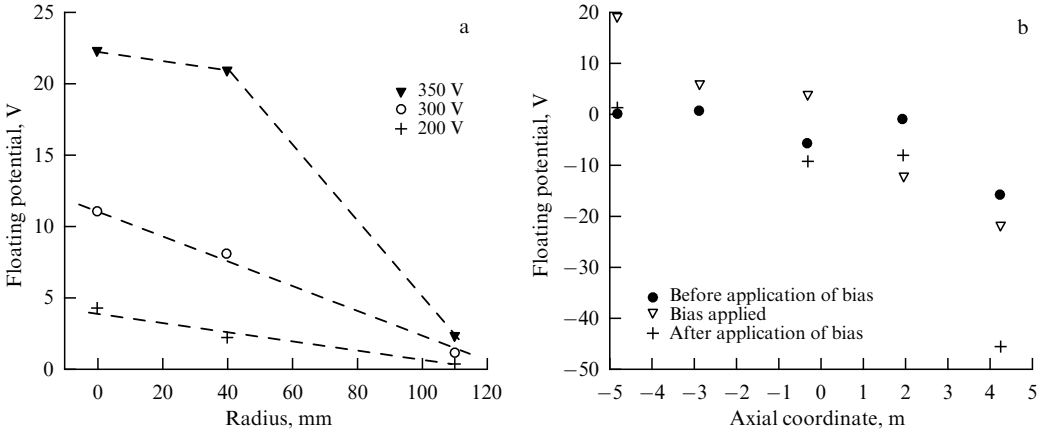

Figure 27. Radial (a) and axial (b) distribution of potential during injection of hydrogen plasma from a helicon source along the axis and positive bias on the end electrode of KMAX installation [59].

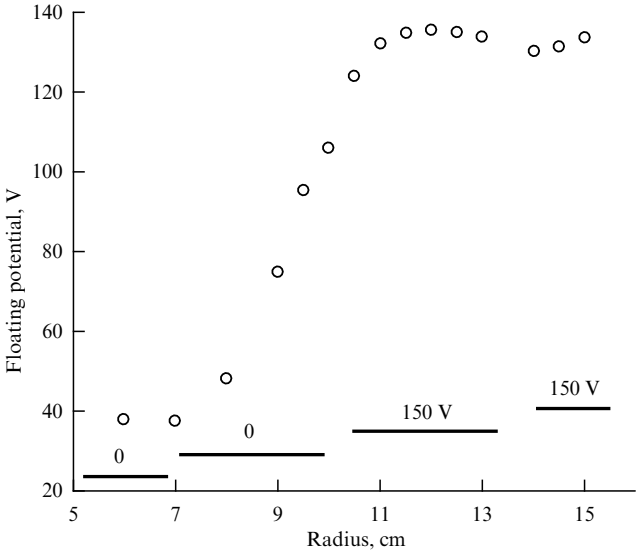

Figure 28. Radial profile of floating potential in central plane of HDT in steady state [121].

first, the collisional target (starting) plasma, had an electron and ion temperature of up to 100 eV and a density of $\sim 5 \times 10^{19}$ m^{-3}. The other component, fast ions with an average energy of 10 keV and a density of up to 2×10^{19} m^{-3}, was created as a result of powerful atomic injection. The estimated level of plasma contact with the end electrodes was 0.2 Ω. If no voltage was applied to the electrodes, they did not affect the MHD stability of plasma confinement, implying that simple contact with the electrodes was not sufficient for MHD stabilization. The plasma confinement time increased significantly when a potential difference of 90–300 V was realized between one or several pairs of biased electrodes, and the electric field was at a level of 1.5–4 kV m^{-1}. In this case, a layer was created with a shear flow (differential rotation) of plasma, where individual layers shifted relative to each other. Figure 28 shows the radial floating potential profile implemented at a bias voltage of 150 V between adjacent electrodes.

Due to the use of a radial electric field, plasma was confined with a record (for this class of installation) target plasma electron temperature of up to 900 eV [122]. The standard method of heating GDT, the total power of which is 5 MW, is atomic injection, while the electron temperature does not exceed 300 eV. Additional heating was implemented by the ECR technique using a 0.7-MW generator, as a result of which the temperature of the electrons was increased. To effectively confine such a plasma, it was necessary to further increase the limiter bias potential from 150 to 300 V [123]. Two schemes for creating a radial electric field were used. In the first one, a positive bias relative to the ground was applied to the limiter, while, in the second scheme, the end electrodes in the paraxial region were maintained at a negative bias [124]. Both schemes suppressed radial losses, but in the latter case the level of MHD activity was significantly lower.

It should be noted that systems that enable control of plasma rotation by applying voltage to a limiter or plasma receiver are becoming 'must-have' elements of all large installations [125].

The data presented can be summarized using the following chain of reasoning. Before the use of end electrodes, the radial distribution of the plasma potential was set due to the balance of longitudinal losses of charged particles [126, 127]. Such losses correlate with the temperature of the electrons. As a first approximation, it can be assumed that losses occur at each radius independently; therefore, the plasma potential distribution corresponds to the electron temperature distribution. If the temperature profile peaks on the axis, the electron temperature gradient generates a force directed from the center. This results in azimuthal rotation, which generates instabilities. The use of end electrodes with an electric field directed towards the axis compensates for this effect and enhances stability [124]. If voltage at the end electrodes is increased further, azimuthal rotation occurs in the opposite direction, which does not lead to MHD instabilities, since the radial force is directed towards the axis. The results of experiments using the GDT apparatus were systematized in review [128].

Creation of a hot starting plasma in the end system of an ambipolar trap was studied at the AMBAL-M installation (ambipolar adiabatic trap) operated by the Institute of Nuclear Physics, Siberian Branch, Russian Academy of Sciences [129]. The plasma was created by an annular source. When the plasma flow is transported, a plasma potential distribution is formed, which is equal in order of magnitude to the cathode-anode potential difference. Such a radial field led to the development of low-frequency instability, apparently associated with the Kelvin–Helmholtz instability [130]. The electrostatic oscillations induced by

Table 4. Consolidated table of parameters of experiments on open traps with an additional ionization source and a potential bias of end electrodes.

Installation	Source	U_e, V	U_{pl}, V	E, V m^{-1}	B, mT	n_p, m^{-3}	A	T_e, eV	T_i, eV	t, ms	N	L, m D, m	Plasma creation method	Method of plasma potential measurement
Phaedrus	[57, 113, 114]	1. −120 2. +60	1. −4 2. +30	1400	66 (7)	2×10^{18}	H	15–20	30	10	4 (2)	$L = 10$ $D = 0.34$	RF heating ($\omega_{rf} = 0.8\omega_{Ci}$)	Floating probe
Gamma 10	[58, 136]	1. −2000 2. +750	1. −200 2. +2200	—	400 (5)	10^{18}	H	60–120	500–800	35	5 (2)	$L = 27$ $D = 0.40$	ECR $f = 28$ GHz	1. Probing with a beam of Au atoms [118] 2. Ion energy analysis
KMAX	[59]	−30 +350	+22	250	15	10^{17}	H	—	—	—	2 (1)	$L = 10$ $D = 0.15$	RF helicon $P = 1.5-2$ kW; $f = 13.56$ MHz	Floating probe
HDT	[56, 137]	1. −150 2. −300	−130	4000	200 (33)	5×10^{19}	H, D	1. < 100 2. 660	10^4	4	4 (2)	$L = 7$ $D = 0.3$	1. Atomic injection $P = 4$ MW; $E = 17$ keV 2. With additional ECR heating	Floating probe
C-2W	[133]	−5000	—	10,000	100–300	2×10^{19}	H, D	300	1000	30	4	$L = 20$ $D = 1.0$	Atomic injection $P = 20$ MW; $E = 15$ keV	Floating probe

Designations: U_e — maximum (in absolute value) potential at end electrodes; U_{pl} — maximum (in absolute value) plasma potential; E — electric field; B — magnetic field is indicated at center of the chamber on the axis. Mirror ratio is given in parentheses; n_p — plasma density; A — symbol notation of the working gas, T_e, T_i — temperature of electrons and ions; t — duration of experiment; N — number of electrodes at one end, figure in parentheses indicates number of groups of electrodes that were under different potentials; L — distance between ends; and D — diameter of discharge cell.

this instability led to heating of the ions and subsequent heating of the electrons.

The considered mechanism of plasma stabilization by differential rotation turned out to be so effective that next-generation open traps also assume this method is used [125, 126].

C-2 type installations (Tri Alpha Energy Inc., USA) [131–133] employ a 'field reversed configuration (FRC).' The use of end electrodes to create radial electric fields resulted in azimuthal rotation of the axisymmetric plasma, which, in turn, provided its stabilization, heating, and growth confinement time. In [131], a radial shear flow was created due to a negative bias of the starting plasma source located on the axis of the apparatus of up to a potential of −450 V; a layer was formed locally with an electric field directed to the axis at the level of 1 kV m^{-1}.

Although this review covers systems with an axial magnetic field, several installations with a more complex magnetic field topology, in which end electrodes were used to control the plasma potential, should nevertheless be mentioned, including SMOLA (spiral magnetic open trap) with multi-mirror traps (Institute of Nuclear Physics, Siberian Branch, Russian Academy of Sciences) [134] and GOL NB (corrugated open trap) [135].

Table 4 presents consolidated parameters of experiments on open traps with an additional ionization source and with a bias in the potential of the end electrodes.

4.3 Q_T-Upgrade machine

One of the most successful studies in what regards controlling the plasma potential by means of end electrodes is an experiment carried out on the Q_T-Upgrade machine (Department of Electronic Engineering, Tohoku University, Japan) [138–140]. This installation is a mirror machine with a mirror ratio of 2.88. In this study, in a cylindrical chamber about 5 m in length and 0.2 m in diameter, concentric segmented end electrodes were located at two ends, three electrodes on each side (Fig. 29a). Argon plasma was created by a microwave discharge with a power of 100–500 W; its density was about 10^{16} m^{-3}.

Configurations for connecting end electrodes were studied with an electric field directed both towards the system axis and away from the axis. Figures 29b, c show the distributions of potential and plasma density at various biases at the end electrodes. In these figures, $\phi_T(\alpha/\beta/\gamma)$ denotes the bias potential at the inner, middle, and outer electrodes (α, β, and γ, respectively). Figure 29b clearly shows that, although the plasma potential is everywhere higher than the bias potential, nevertheless, the shape of the potential at a qualitative level corresponds to the voltage applied to the end electrodes. The plasma potential being higher than the potential of the end electrodes indicates the presence of a near-electrode sheath.

A comparison of Fig. 29b, c shows that, with an increase in the electric field directed from the center, the plasma density begins to decrease, while the radial current increases (Fig. 29d). This can be explained by the fact that the precession frequency of the ion orbit at $E_r > 200$ V m^{-1} approaches the Brillouin limit for confining charged particles in crossed fields [141].

4.4 Plasma mass separation

As noted in the Introduction, control of the radial profile of the plasma potential is extremely important for plasma mass

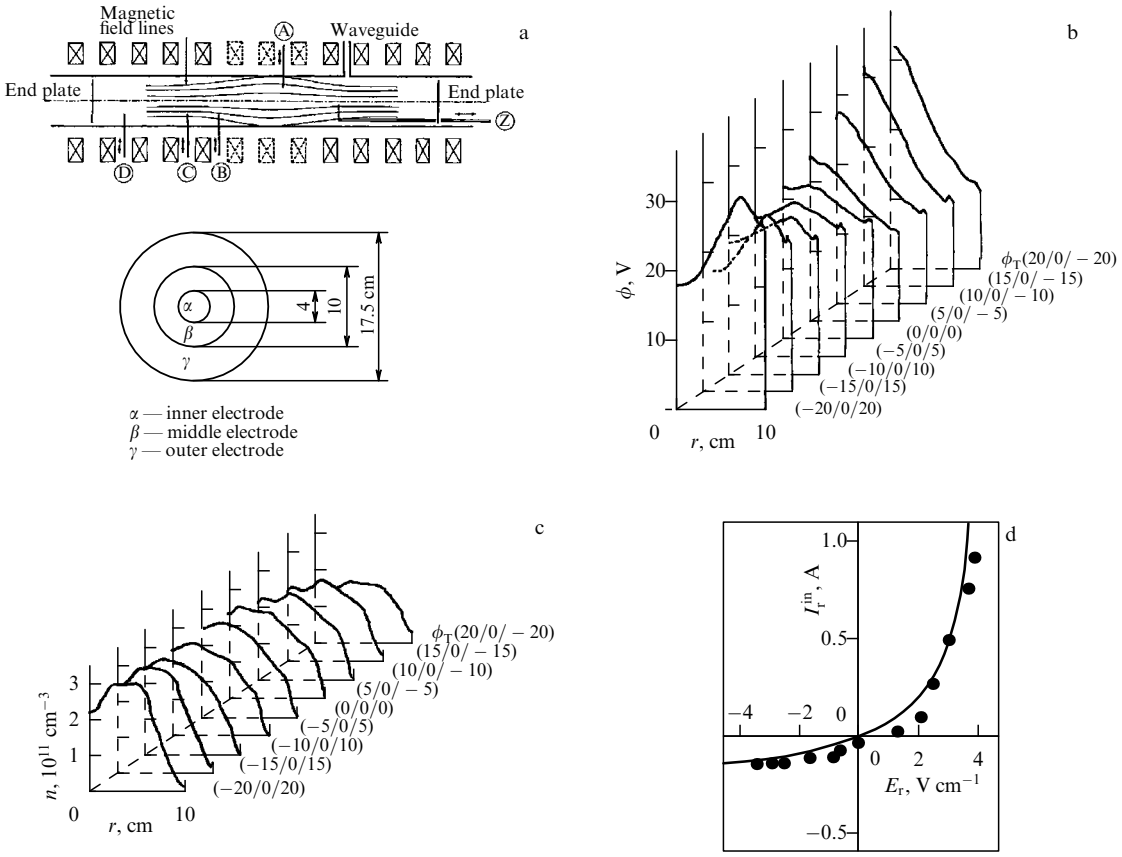

Figure 29. Setup of experimental installation and end electrodes of Q_T-Upgrade machine (a); radial distributions of potential (b); and plasma density (c) as a function of the voltage applied to the end electrodes; dependence of the radial current I_r^{in} on the radial electric field E_r (d). © (1991) The Physical Society of Japan [139].

separation methods. Initially, these methods were intended to separate various isotopes of chemical elements [142]. Recently, the feasibility of applying them for a coarser separation of groups of chemical elements has been considered. For example, to reprocess spent nuclear fuel, it may be useful to separate rare earth elements with an atomic mass lighter than 150 a.m.u. from minor actinides heavier than 235 a.m.u.

One of the research team conducting studies in this area was Archimedes Technology Group (a private company). It developed the concept of an ion mass filter, based on the specific features of the movement of particles in a plasma with magnetized electrons and a parabolic axisymmetric potential realized in the plasma volume [16]. The separation scheme is shown in Fig. 30. The particles being separated are injected into the center of the system, where they start moving under the effect of electric and magnetic fields. As a result, heavier particles, the mass of which exceeds the critical mass $m_c = ZeB^2R^2/8V_0$ [SI] (V_0 is the plasma potential on the axis of the system with a parabolic distribution of the plasma potential), are ejected onto collectors located on the cylindrical surface of the installation, while lighter particles remain in the plasma volume and then move to collectors located at the ends of the device.

A number of important results in creating a radial electric field in plasma were obtained using the DEMO (Archimedes) installation developed by Archimedes Technology Group, USA [143]. The plasma column was created by RF antennas; the discharge power was about 700 kW with a magnetic field

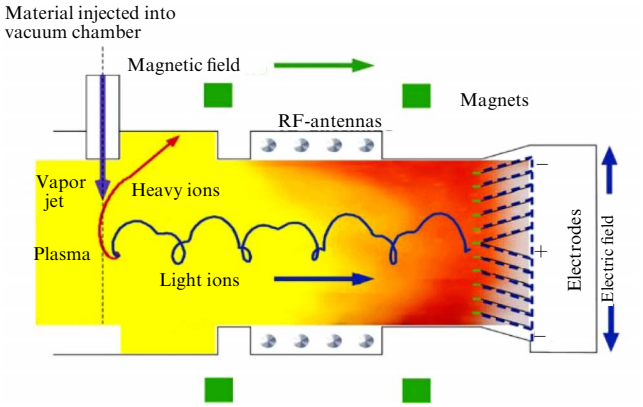

Figure 30. Mass separation at the DEMO installation (Archimedes) [145].

of 0.09 T. The density of sodium plasma was 4×10^{18} m^{-3}, and that of argon plasma was 10^{19} m^{-3}. It was shown that a positive bias at the end electrodes can be used to create a parabolic potential profile [144]. Moreover, if metal vapors are used as a plasma-forming gas, the plasma potential distribution coincides well with the smoothed distribution of the end electrode potential. If an inert gas plasma is used, there is no electric field at the column periphery, and a 'flat region' is formed. The density profile in sodium plasma remains flat, while in argon plasma it becomes 'hollow.' Before the end electrodes in the argon plasma were turned on, the density profile was also flat.

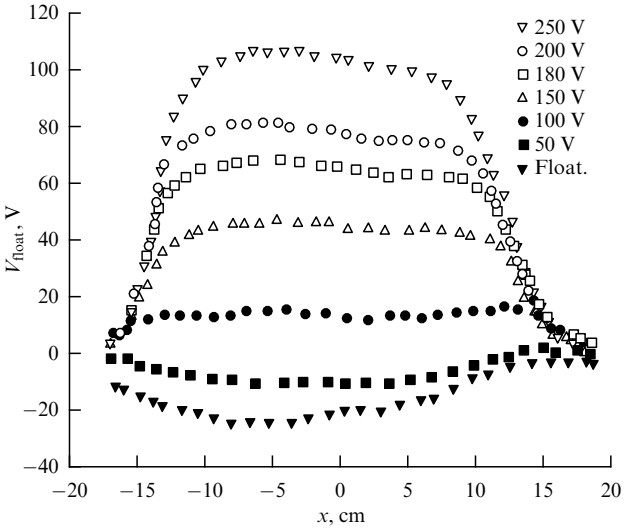

Figure 31. Radial profile of the floating potential on the installation [146].

This difference in the behavior between metal plasma and the plasma of inert gases is explained primarily by the accumulation of neutral atoms of inert gases at the discharge periphery, while metal atoms are deposited on chamber walls.

A similar method for separating chemical elements was tested in Ref. [146]. The RF antenna for plasma generation was located at one end of a cylindrical chamber 1.7 m in length and 0.445 m in diameter, and an assembly of 10 concentric electrodes designed to create a potential in the plasma volume was located at the other end. The antenna power was 160 W, and the operating frequency was 7 MHz. Ar, Xe, and Kr were used as plasma-forming gases at a pressure of ~ 0.013 Pa. The plasma density was $(0.3-1.4) \times 10^{16}$ m^{-3}; the magnetic field was about 0.12 T. A positive bias was applied to the outer three electrodes, and the inner electrodes were maintained under a floating potential. Figure 31 shows that the potential response to an increase in the positive bias applied to electrodes 8–10 is clearly observed, although the level of the floating potential is significantly lower than the potential of the end electrodes. If lighter Ar gas was substituted with heavier Kr, the level of floating potential decreased further.

One more experiment of a plasma mass filtering is presented in Ref. [147]. In this work the properties of helicon plasma and the effect of confining argon and krypton ions were studied. To create a radial electric field, a movable set of three concentric electrodes was used, located at only one end of the installation with a length of ~ 0.8 m and a variable diameter from 0.60 to 0.15 m. At the opposite end, an RF antenna (800 W, 13.6 MHz) was located. The magnetic field on the axis was about 0.95 kG. The pressure of the working gas, a mixture of nitrogen, argon, krypton, and helium, was 0.7 Pa. The plasma density was on the level of 10^{18} m^{-3}. Various potentials of relatively small magnitude ranging from -35 to $+40$ V were applied to the end electrodes. Experiments showed that only a positive potential was reproduced in the plasma volume, the maximum value of which was $+20$ V at an electric field of 500 V m^{-1}.

In [148], reproduction of the electric potential in a plasma volume was studied as part of the development of a plasma separation scheme with a potential well [6, 17, 149]. Separation in this scheme occurs in a plane perpendicular to the magnetic field, in the electric potential of a special configuration. A specific feature of this approach is the use of the accelerating potential to suppress the energy and angular spread of substance ion plasma at the entrance to the separator chamber and a potential well for the spatial separation of ions of different masses. The trajectories of the ions are such that the created potential effectively captures heavy ions and barely affects light ones.

In a concept of plasma separation with a potential well implemented at the LaPlaS installation (Joint Institute for High Temperatures of the Russian Academy of Sciences, Russia), a background plasma is created separately, and a specified spatial distribution of the potential is realized in this plasma. Separately, a plasma of separated substances is created, which is injected into the background plasma. The ions of the substances being separated are entrained by the electric field of the background plasma and spatially separated by mass. In [148], plasma was created by an RF discharge in a cylindrical chamber with a diameter of 0.86 m and a length of 2.3 m in an argon atmosphere at a pressure of 0.7 Pa. The magnetic field, which was created by Helmholtz coils, was at a level of 0.065 T. The maximum plasma density was 2×10^{18} m^{-3}. Electrodes with a diameter of 0.45 m were located at both ends. A negative bias was applied to the electrodes. An increase in the negative bias at the electrode to -75 V led to a decrease in the plasma potential (Fig. 32a), resulting in a change in the plasma density profile and electron temperature (Fig. 32b, c). On the one hand, the maximum density decreased, and on the other hand, the density on the discharge axis increased. An increase in the negative bias above -30 V led to a mismatch between the RF generator and the plasma; therefore, in the mode with a more negative bias, the absorbed RF power was significantly lower. An even more negative bias, < -75 V, of the end electrode did not lead to a decrease in the plasma potential. This phenomenon is explained in [36], where it is shown that, in this geometry at a pressure of 0.7 Pa and a magnetic field of 0.065 T, there is a limitation on the negative potential of the plasma.

The negative potential reproduced in the plasma volume can be significantly reduced by adding a source of thermionic emission to the end electrodes. A noticeable effect of introducing an additional source of charged particles on the reproduction of the potential is also observed in other studies reviewed here (see Tables 2 and 4).

A series of studies conducted to explore plasma separation in a reflex discharge [150, 151] highlighted the important role of the injection of charged particles in creating the potential distribution in the plasma volume. In [150], the mutual influence of the plasma beam and the background plasma into which the beam was injected was experimentally studied, and the resulting distortions in the spatial distribution of the electric potential in the plasma volume were examined. The conceptual setup and parameters of the experiment are presented in Fig. 33a. The background plasma was ignited in an argon atmosphere (pressure 0.05 Pa); the magnetic field $B \sim 0.15$ T; the plasma density in the injected jet was up to 10^{18} m^{-3}; and the voltage at the end electrodes was -1.2 kV.

It was shown that, if a plasma jet was not injected, the characteristic potential and electric field obtained inside the plasma volume were -350 V and 8 kV m^{-1}, while with injection they dropped to -50 V and 1.6 kV m^{-1}, respectively, and below. As a result, it was assumed that the number of magnetized electrons of the background discharge becomes insufficient to compensate for the charge of

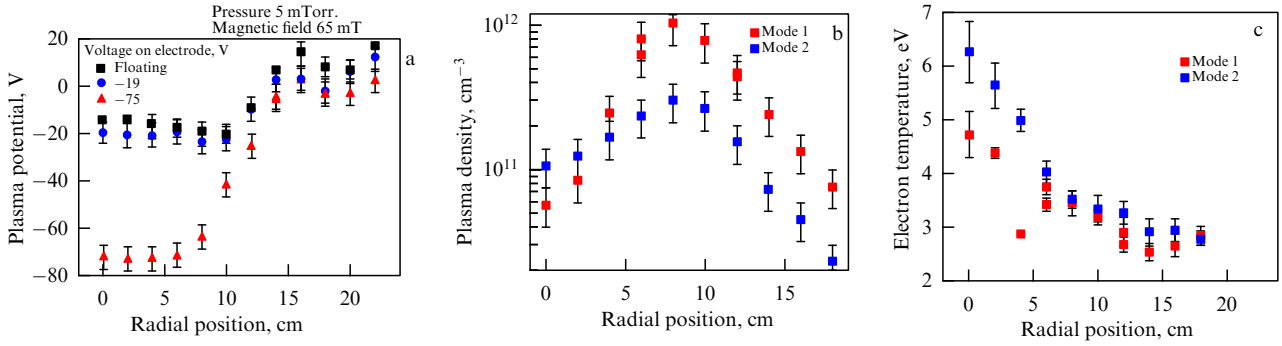

Figure 32. Reproduction of electrical potential of end electrodes in an RF discharge [148]. Radial profile of floating potential (a), plasma density (b), and electron temperature (c).

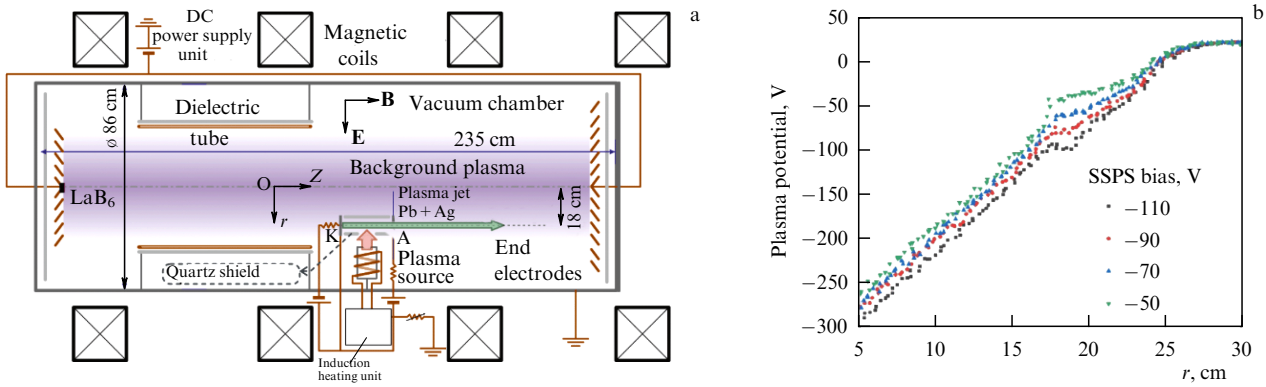

Figure 33. (a) Schematic of an experiment studying the effect of injection of a metal plasma beam on the distribution of electric potential created by end electrodes in background plasma of an inert gas. (b) Influence of plasma injector potential on potential distribution in the separator volume [151].

ions provided by the injected plasma jet, and this changes in the distribution of charges in the plasma volume and significantly distorts the spatial electric potential profile. It was proposed to enhance the injection of electrons into the plasma volume to create a controlled potential profile by arranging additional thermionic emission at the end electrodes. The feasibility of this approach was demonstrated on a modified LaPlaS installation [151], where a system of five concentric end electrodes located at the ends of the discharge chamber was used to generate a potential well and a negative electric potential in the volume of magnetized plasma. At one of the ends, in the center of the electrode assembly, a thermionic element (thermal emission cathode) with a diameter of 2×10^{-2} m was also installed. The first three concentric electrodes, counting from the center, together with the thermionic cathode were galvanically connected to each other and to a power supply, and the remaining electrodes were maintained under a floating potential. The cylindrical walls of the chamber were grounded. Two modes of discharge operation, with a heated and cold thermionic cathode, were studied. In the latter case, a voltage of -1 kV was applied to the electrodes, and the discharge current was 50 mA. The potential in the plasma volume in the mode without additional thermionic emission was -60 V. In the mode with a heated thermionic cathode, the discharge was created by applying a voltage of -550 V, and its current reached 10 A. In this case, the potential of the end electrodes was reproduced in the plasma significantly better and reached a value of -300 V. Also varied in [151] were the conditions for injection of the plasma jet into the volume of the background plasma. It was shown that the potential can be locally varied (both increased and decreased) without disturbing it in the rest of the volume (Fig. 33b). This problem of distortion of the potential distribution, which has not yet been studied in general, is of considerable interest.

As a comment, we note that when preparing and planning any experiments, developing technical devices, and conducting experiments that involve the issues of reproducing the electric potential in a plasma volume, it is useful to have a relatively simple tool that shows the values of the potential that can be expected under the assumed experimental conditions. One such tool for axisymmetric plasma systems with a magnetic field and end electrodes is a series of relationships proposed in [36, 37]. For example, for the geometry presented in Fig. 1 and negative voltage on the end electrodes $U_e \gg T_e$ (temperature of plasma electrons), the distribution $U(r)$ of the potential in the plasma volume is determined by the current density, the flow of which can be provided through plasma and can be calculated using the formula

$$U(r) = \frac{2}{3}\sqrt{C_1 C_2}\,(r^{3/2} - r_g^{3/2})\ [\mathrm{SI}]\,,$$

where

$$C_1 = \frac{0.52}{2e}\,\frac{(MkT_e)^{1/2} n\sigma_{in}}{BL}\,, \quad C_2 = \left(\frac{eB^2}{Mn\sigma_{in}}\right)^2,$$

e is the elementary charge, k is the Boltzmann constant, M is the mass of the atom (ion), n is the density of atoms of the plasma-forming gas, σ_{in} is the cross section of elastic collisions of ions with neutral particles, and B is the induction of an external constant homogeneous magnetic field.

Table 5. Consolidated table of parameters of experiments on plasma mass separation with a bias of end-electrode potential.

Installation	Source	U_e, V	U_{pl}, kV	E, V m^{-1}	B, T	n_p, m^{-3}	p, Pa	T_e, eV	T_i, eV	t, s	N	L, m D, m	Plasma creation method	Method of measurements of plasma potential
DEMO (Archimedes)	[14, 143, 144, 152]	+97	+96	600	0.09	4×10^{18}	Na, Ar 65–70	1–3	—	Cont.	10	$L = 4$ $D = 0.8$	RF inductive discharge 300–500 kW $f = 4$ MHz	1. Floating probe 2. Doppler spectroscopy
Large diameter helicon	[146]	+250	+100	2500	0.12	3×10^{15} 1×10^{16}	Ar, Xe 21	3–6	< 1	Cont.	10 (2)	$L = 1.70$ $D = 0.45$	RF inductive discharge $P_{rf} = 0.16$ kW $f = 7$ MHz	1. Langmuir probe 2. Mach probe
LaPlaS RF	[148]	−200	−70	1000	0.065	5×10^{17}	Ar 665	3–6	—	Cont.	2	$L = 230$ $D = 0.86$	RF inductive discharge $P_{rf} = 0.5$ kW $f = 5$ MHz	Floating probe
LaPlaS Reflex	[37, 151]	−550 Thermal emission cathode	−300	1500	0.14	3×10^{17}	Ar 40	7–9	—	Cont.	5 (2)	$L = 230$ $D = 0.86$	Reflex discharge with hot cathode $I = 10$ A	Emissive probe
PMFX	[147]	−35 +40	+20 +16	500	0.095	10^{19}	Ar, Kr, Ne, N_2, 665	3	0.03	Cont.	3	$L = 0.73$ $D = 0.2$	RF inductive discharge $P_{rf} = 0.8$ kW f=13.56 MHz	Floating probe

Designations: U_e — maximum (in absolute value) potential at end electrodes; U_{pl} — maximum (in absolute value) plasma potential; E — electric field; B — magnetic field is indicated at center of the chamber on the axis. Mirror ratio is given in parentheses; n_p — plasma density; p — neutral gas pressure, T_e, T_i — temperature of electrons and ions; t — duration of experiment; N — number of electrodes at one end: figure in parentheses indicates number of groups of electrodes that were under different potentials; L — distance between ends, and D — diameter of discharge cell. Large diameter helicon — Kyushu University, Japan; PMFX — Plasma Mass Filter experiment, Princeton Plasma Physics Laboratory, Princeton University, USA.

Table 5 presents consolidated data from experiments on plasma mass separation with a potential bias of end electrodes.

5. Conclusions

An analysis of experimental studies has shown that the use of end electrodes in axial plasma systems with a longitudinal magnetic field enables the distribution of the transverse electric field to be controlled. For such control, the condition of electron magnetization is not sufficient. A list of the factors affecting the absolute value and distribution of the electric potential reproduced in the plasma volume includes the magnetic field, the voltage applied to the electrodes, the type of plasma-forming gas and its pressure, and the geometry of the electrodes (their surface area, relative position, potential distribution on them). Some studies note the influence on the electric field shape of the degree of electrode surface treatment and their material.

The task to create potential distribution with local maximum inside the plasma is significantly differ from the task to create potential distribution with local minimum. For example, the case when the plasma column potential is higher than the potential of the cylindrical chamber (i.e., the plasma column has a positive volume charge) can be implemented relatively simply. This is due to the fact that, since the mobility of electrons along the magnetic field lines is higher than that of ions, for typical experimental geometries, the active escape of negative electric charge from the plasma volume through the end electrodes is automatically ensured.

To create negative potentials in a plasma volume comparable to the voltage applied to the end electrodes (i.e., when the plasma column has a negative volume charge), it is necessary to ensure either the removal of positive charge from the plasma volume by an ion current or an additional influx of negative charge due to the injection of electrons. Each of these options can in principle be implemented. One of the simplest ways to create negative potentials is, apparently, the use of thermionic emission from the end electrodes. It should be noted that a number of studies have also shown that plasma rotation can be stabilized using this method. In addition, in problems related to plasma mass separation, the introduction of an additional negative charge makes it possible to compensate for the positive charge of the ions of the substances being separated and to eliminate a number of restrictions on the efficiency of this method.

Most of the presented studies were with one local minimum or maximum of the potential. Nevertheless, some experimental studies have shown that more complex stationary distributions of the electric potential in the plasma volume — containing several local extrema — can be formed. The issue of the accuracy with which the potential distribution of the electrodes can be reproduced in the plasma volume remains open in terms both of spatial fineness and fluctuations in average values.

The results of experiments helped to validate analytical model which predicts the potential distribution in the system with negative potential on the axis. This model takes into account the transverse conductivity of the plasma, the near-cathode potential drop, and the potential drop due to the flow of thermionic current from the electrodes and are an efficient

aid to experimenters in choosing experimental parameters and analyzing the results obtained.

The choice of the diagnostic tools is also very important. In the analyzed studies, various probe methods were used, in particular, the methods of floating and emissive probes. The difference in the results of measurements made by these methods in most cases is on the order of the plasma electron temperature, but this assertion is only true in the case of a Maxwellian electron energy distribution. The requirement for the shape of the distribution function is fairly stringent, as a result of which significant differences can arise in some cases between the values of the plasma potential obtained using a floating and a emissive probe. The authors of the review recommend using in experiments the thermionic probe method, which, although more technically complex, is more reliable.

Acknowledgments. The study was supported by the Russian Science Foundation (grant no. 21-19-00716, https://rscf.ru/proj ect/21-19-00716/).

References

1. Dolgolenko D A, Muromkin Yu A *Phys. Usp.* **60** 994 (2017); *Usp. Fiz. Nauk* **187** 1071 (2017)
2. Zweben S J, Gueroult R, Fisch N J *Phys. Plasmas* **25** 090901 (2018)
3. Paperny V L et al. *Plasma Sources Sci. Technol.* **24** 015009 (2015)
4. Bardakov V M, Ivanov S D, Strokin N A *Phys. Plasmas* **21** 033505 (2014)
5. Zhil'tsov V A et al. *Atom. Energy* **101** 755 (2006); *At. Energ.* **101** (4) 302 (2006)
6. Liziakin G et al. *Plasma Phys. Control. Fusion* **63** 032002 (2021)
7. Timofeev A V *Phys. Usp.* **57** 990 (2014); *Usp. Fiz. Nauk* **184** 1101 (2014)
8. Yuferov V B et al. *Problems Atom. Sci. Technol.* **107** (1) 223 (2017)
9. Gueroult R, Fisch N J *Plasma Sources Sci. Technol.* **23** 035002 (2014)
10. Gueroult R, Rax J-M, Fisch N J *J. Cleaner Product.* **182** 1060 (2018)
11. Dolgolenko D A, Muromkin Yu A *Phys. Usp.* **52** 345 (2009); *Usp. Fiz. Nauk* **179** 369 (2009)
12. Borisevich V D, Potanin E P, Whichello J *Phys. Plasmas* **25** 113503 (2018)
13. Dolgolenko D A, Muromkin Yu A, Pashkovsky V G *Instrum. Exp. Tech.* **62** 798 (2019); *Prib. Tekh. Eksp.* (6) 60 (2019)
14. Freeman R et al. *AIP Conf. Proc.* **694** 403 (2003)
15. Gueroult R et al. *Phys. Plasmas* **26** 043511 (2019)
16. Ohkawa T, Miller R L *Phys. Plasmas* **9** 5116 (2002)
17. Smirnov V P et al. *Plasma Phys. Rep.* **39** 456 (2013); *Fiz. Plazmy* **39** 523 (2013)
18. Lieberman M A, Lichtenberg A J *MRS Bull.* **30** 899 (1994)
19. Raizer Yu P *Gas Discharge Physics* (Berlin: Springer, 1997); Translated from Russian: *Fizika Gazovogo Razryada* (Dolgoprudnyi: Intellekt, 2009)
20. Baalrud S D et al. *Plasma Sources Sci. Technol.* **29** 053001 (2020)
21. Morozov A I *Introduction to Plasma Dynamics* (Boca Raton, FL: CRC Press, 2012); Translated from Russian: *Vvedenie v Plazmodinamiku* (Moscow: Fizmatlit, 2008)
22. Abolmasov S N *Plasma Sources Sci. Technol.* **21** 035006 (2012)
23. Hooper E B (Jr.), in *Advances in Electronics and Electron Physics* Vol. 27 (Eds L Marton, C Marton) (Amsterdam: Elsevier, 1970) p. 295
24. Villafana W et al. *Plasma Sources Sci. Technol.* **30** 075002 (2021)
25. Kaganovich I D et al. *Phys. Plasmas* **27** 120601 (2020)
26. Garbet X et al. *Nucl. Fusion* **50** 043002 (2010)
27. Winske D et al., in *Space Plasma Simulation* (Lecture Notes in Physics, Vol. 615, J Büchner, C Dum, M Scholer) (Berlin: Springer, 2003) p. 136
28. Taccogna F et al. *Phys. Plasmas* **12** 053502 (2005)
29. Taccogna F et al. *AIP Conf. Proc.* **1501** 1390 (2012)
30. Charoy T et al. *Plasma Sources Sci. Technol.* **28** 105010 (2019)
31. Boeuf J-P, Chaudhury B *Phys. Rev. Lett.* **111** 155005 (2013)
32. Boeuf J-P *J. Appl. Phys.* **121** 011101 (2017)
33. Jorns B A et al. *Phys. Plasmas* **27** 022311 (2020)
34. Carlsson J et al. *Phys. Plasmas* **25** 061201 (2018)
35. Smolyakov A I et al. *Plasma Phys. Control. Fusion* **59** 014041 (2017)
36. Liziakin G, Gavrikov A, Smirnov V *Plasma Sources Sci. Technol.* **29** 015008 (2020)
37. Liziakin G et al. *J. Plasma Phys.* **87** 905870414 (2021)
38. Burrell K H *Phys. Plasmas* **4** 1499 (1997)
39. Itoh K, Itoh S-I *Plasma Phys. Control. Fusion* **38** 1 (1996)
40. Chandrasekhar S *Hydrodynamic and Hydromagnetic Stability* (New York: Dover Publ., 2013)
41. Lehnert B *Nucl. Fusion* **11** 485 (1971)
42. Klopfer A *Vakuum-Tech.* **10** 113 (1961)
43. Schuurman W *Physica* **36** 136 (1967)
44. Gabovich M D, Bartnovskii O A, Fedorus Z P *Sov. Phys. Tech. Phys.* **5** 320 (1960); *Zh. Tekh. Fiz.* **30** 345 (1960)
45. Liziakin G D et al. *Phys. Plasmas* **23** 123502 (2016)
46. Rohwer P et al. *Nucl. Instrum. Meth. Phys. Res.* **211** 543 (1983)
47. Smirnitskaya G V, Ti N Kh *Sov. Phys. Tech. Phys.* **14** 783 (1969); *Zh. Tekh. Fiz.* **39** 1044 (1969)
48. Kim J Y et al. *AIP Adv.* **11** 085113 (2021)
49. Baumann H, Bethge K *Nucl. Instrum. Meth.* **122** 517 (1974)
50. Rohwer P et al. *Nucl. Instrum. Meth. Phys. Res.* **204** 245 (1982)
51. Abdrashitov G F et al. *Nucl. Fusion* **31** 1275 (1991)
52. Bekhtenev A A et al. *Nucl. Fusion* **20** 579 (1980)
53. Bekhtenev A A, Volosov V I *Sov. Phys. Tech. Phys.* **23** 938 (1978); *Zh. Tekh. Fiz.* **48** 1657 (1978)
54. Bocharov V N et al. *Sov. J. Plasma Phys.* **4** 271 (1978); *Fiz. Plazmy* **4** 488 (1978)
55. Konstantinov S G et al. *Sov. Phys. Tech. Phys.* **16** 2006 (1972); *Zh. Tekh. Fiz.* **41** 2527 (1971)
56. Bagryansky P A, Beklemishev A D, Soldatkina E I *Fusion Sci. Technol.* **51** 340 (2007)
57. Hershkowitz N et al. *Plasma Phys. Control. Nucl. Fusion Res.* **2** 265 (1984)
58. Mase A et al. *Nucl. Fusion* **31** 1725 (1991)
59. Zhang Q et al. *Fusion Sci. Technol.* **68** 50 (2015)
60. Volosov V I *Plasma Phys. Rep.* **35** 719 (2009); *Fiz. Plazmy* **35** 782 (2009)
61. Rosenbluth M N, Simon A *Phys. Fluids* **8** 1300 (1965)
62. Bogdanov G F et al. *Nucl. Fusion Suppl.* **1** 215 (1962)
63. Kunkel W B, Guillory J U, in *Phenomena in Ionized Gases. Proc. of the Seventh Intern. Conf., August 22–27, 1965, Beograd, Yugoslavia* Vol. 2 (Eds B Perović, D Tošić) (Beograd: Gradevinska Knjiga Publ. House, 1966) p. 702
64. Lehnert B *Phys. Scr.* **7** 102 (1973)
65. Prater R *Phys. Fluids* **17** 193 (1974)
66. Timofeev A V *Nucl. Fusion* **6** 93 (1966)
67. Bekhtenev A A, Vandegrift G G, Volosov V I *Sov. J. Plasma Phys.* **14** 168 (1988); *Fiz. Plazmy* **14** 292 (1988)
68. Bekhtenev A A, Volosov V I *Sov. Phys. Tech. Phys.* **22** 834 (1977); *Zh. Tekh. Fiz.* **47** 1450 (1977)
69. Spies G O *Phys. Fluids* **21** 580 (1978)
70. Timofeev A *Resonance Phenomena in Plasma Oscillation* (*Plasma Physics*) (London: Taylor and Francis, 2010); *Rezonansnye Yavleniya v Kolebaniyakh Plazmy* (Moscow: Fizmatlit, 2009)
71. Abdrashitov G F et al. *Vopr. Atom. Nauki Tekh. Ser. Termoyad. Sintez* (1) 54 (1988)
72. Volosov V I et al. *Priklad. Fiz.* (4) 22 (2000)
73. Konstantinov S G, Tsel'nik F A *Sov. Phys. Tech. Phys.* **16** 382 (1971); *Zh. Tekh. Fiz.* **41** 493 (1971)
74. Abdrashitov G F et al., in *8th Intern. Conf. on Plasma Physics and Controlled Nuclear Fusion Research, Brussels, 1–10 July 1980* (Brussels: IAEA, 1980) p. 539
75. Motley R W *Q Machines* (New York: Academic Press, 2012)
76. Rynn N, D'Angelo N *Rev. Sci. Instrum.* **31** 1326 (1960)
77. D'Angelo N, Motley R W *Phys. Fluids* **6** 422 (1963)
78. Jassby D L, Perkins F W *Phys. Rev. Lett.* **24** 256 (1970)
79. Kent G I, Jen N C, Chen F F *Phys. Fluids* **12** 2140 (1969)
80. Enriques L, Levine A M , Righetti G B *Plasma Phys.* **10** 641 (1968)
81. Jassby D L *Phys. Fluids* **15** 1590 (1972)
82. Ganguli G, Lee Y C, Palmadesso P *Phys. Fluids* **28** 761 (1985)

83. Koepke M E, Amatucci W E *IEEE Trans. Plasma Sci.* **20** 631 (1992)
84. Schrittwieser R *Phys. Fluids* **26** 2250 (1983)
85. Carroll J J (III) et al. *Rev. Sci. Instrum.* **65** 2991 (1994)
86. Koepke M E et al. *Phys. Rev. Lett.* **72** 3355 (1994)
87. Bowles J H et al. *Rev. Sci. Instrum.* **67** 455 (1996)
88. Amatucci W E et al. *Phys. Rev. Lett.* **77** 1978 (1996)
89. Lynn A G et al. *Rev. Sci. Instrum.* **80** 103501 (2009)
90. Gilmore M et al. *J. Plasma Phys.* **81** 345810104 (2015)
91. Desjardins T R, Gilmore M *Phys. Plasmas* **23** 055710 (2016)
92. Desjardins T R, Gilmore M *Phys. Plasmas* **25** 062117 (2018)
93. Gilmore M et al., in *Proc. of the 36th EPS Conf. on Plasma Physics 2009, Sofia, Bulgaria, 29 June – 3 July 2009* (Europhysics Conf. Abstracts, Vol. 33E, Eds M Mateev, E Benova) (Mulhouse: EPS, 2009) p. 85
94. Gilmore M et al., in *Proc. of the 38th EPS Conf. on Plasma Physics 2009, Strasbourg, France, 27 June – 1 July 2011* (Europhysics Conf. Abstracts, Vol. 35G, Eds A Becoulet et al.) (Mulhouse: EPS, 2012) p. 660
95. Murzaev Ya et al. *Plasma Sci. Technol.* **21** 045401 (2019)
96. Leneman D, Gekelman W, Maggs J *Rev. Sci. Instrum.* **77** 015108 (2006)
97. Carter T A, Maggs J E *Phys. Plasmas* **16** 012304 (2009)
98. Maggs J E, Carter T A , Taylor R J *Phys. Plasmas* **14** 052507 (2007)
99. Schaffner D A et al. *Phys. Rev. Lett.* **109** 135002 (2012)
100. Jin S et al. *Phys. Plasmas* **26** 022105 (2019)
101. Désangles V et al. *J. Plasma Phys.* **87** 905870308 (2021)
102. Pagaud F et al., in *Proc. of the 48th EPS Conf. on Plasma Physics, EPS 2022, 27 June – 1 July 2022, Online* (Europhysics Conf. Abstracts, Vol. 46A, Eds T Klinger et al.) (Mulhouse: EPS, 2022) p. 985
103. Groebner R J, Burrell K H, Seraydarian R P *Phys. Rev. Lett.* **64** 3015 (1990)
104. Ida K et al. (JFT-2M Group) *Phys. Rev. Lett.* **65** 1364 (1990)
105. Ritz Ch P et al. *Phys. Rev. Lett.* **65** 2543 (1990)
106. Taylor R J et al. *Phys. Rev. Lett.* **63** 2365 (1989)
107. Berkowitz J, Grad H, Rubin H, in *Proc. of the 2nd United Nations Intern. Conf. on the Peaceful Uses of Atomic Energy, Geneva, Switzerland, 1–13 September 1958* Vol. 31 (Geneva: United Nations, 1958) p. 177
108. Fornaca S, Kiwamoto Y, Rynn N *Phys. Rev. Lett.* **42** 772 (1979)
109. Dimov G I *Phys. Usp.* **48** 1129 (2005); *Usp. Fiz. Nauk* **175** 1185 (2005)
110. Post R F et al. *Fusion Sci. Technol.* **47** 49 (2005)
111. Dimov G I, Zakaidakov V V, Kishinevskii M E *Sov. J. Plasma Phys.* **2** 326 (1976); *Fiz. Plazmy* **2** 597 (1976)
112. Fowler T K, Logan B G *Comments Plasma. Phys. Control. Fusion* **2** 167 (1977)
113. Severn G D et al. *Phys. Fluids B* **3** 114 (1991)
114. Severn G D, Hershkowitz N *Phys. Fluids B* **4** 3210 (1992)
115. Enriques L, Garosi F, Neri A, in *Proc. of the Conf. on Physics of Quiescent Plasmas, Frascati, 10–13 January 1967* Vol. 10 (1967) p. 627
116. Schrittwieser R et at. *Plasma Phys. Control. Fusion* **26** 1591 (1984)
117. Rynn N *Rev. Sci. Instrum.* **35** 40 (1964)
118. Ishii K et al. *Nucl. Fusion* **30** 1051 (1990)
119. Mase A et al. *Phys. Rev. Lett.* **64** 2281 (1990)
120. Bagryansky P A et al. *Fusion Sci. Technol.* **43** 152 (2003)
121. Beklemishev A D et al. *Fusion Sci. Technol.* **57** 351 (2010)
122. Bagryansky P A et al. *Phys. Rev. Lett.* **114** 205001 (2015)
123. Bagryansky P A et al. *Nucl. Fusion* **55** 053009 (2015)
124. Yakovlev D V et al. *Nucl. Fusion* **58** 094001 (2018)
125. Endrizzi D et al. *J. Plasma Phys.* **89** 975890501 (2023)
126. Skovorodin D I et al. *Plasma Phys. Rep.* **49** 1039 (2023); *Fiz. Plazmy* **49** 831 (2023)
127. Soldatkina E I et al. *Nucl. Fusion* **60** 086009 (2020)
128. Ivanov A A, Prikhodko V V *Phys. Usp.* **60** 509 (2017); *Usp. Fiz. Nauk* **187** 547 (2017)
129. Akhmetov T D et al. *Plasma Phys. Rep.* **23** 911 (1997); *Fiz. Plazmy* **23** 988 (1997)
130. Kabantsev A A, Taskaev S Yu *Sov. J. Plasma Phys.* **16** 406 (1990); *Fiz. Plazmy* **16** 700 (1990)
131. Tuszewski M et al. (The TAE Team) *Phys. Rev. Lett.* **108** 255008 (2012)
132. Tuszewski M *Nucl. Fusion* **28** 2033 (1988)
133. Gota H et al. *Nucl. Fusion* **61** 106039 (2021)
134. Inzhevatkina A A et al. *Plasma Phys. Rep.* **47** 794 (2021); *Fiz. Plazmy* **47** 706 (2021)
135. Postupaev V V et al. *Nucl. Fusion* **62** 086003 (2022)
136. Cho T et al. *Phys. Rev. Lett.* **94** 085002 (2005)
137. Soldatkina E I, Bagryansky P A, Solomakhin A L *Plasma Phys. Rep.* **34** 259 (2008); *Fiz. Plazmy* **34** 291 (2008)
138. Tsushima A et al. *Phys. Rev. Lett.* **56** 1815 (1986)
139. Tsushima A, Sato N *J. Phys. Soc. Jpn.* **60** 2665 (1991)
140. Yoshinuma M et al. *Phys. Lett. A* **255** 301 (1999)
141. Oiler A P et al. *Tech. Phys.* **67** 1327 (2022); *Zh. Tekh. Fiz.* **92** 1529 (2022)
142. Grossman M W, Shepp T A *IEEE Trans. Plasma Sci.* **19** 1114 (1991)
143. Cluggish B P et al. *Phys. Plasmas* **12** 057101 (2005)
144. Cluggish B P, in *47th Annual APS Division of Plasma Physics Meeting Abstracts, October 24–28, 2005* Vol. 47 (College Park, MD: American Physical Society, 2005) p. KP1-075
145. Gilleland J et al., in *Waste Management Conf., Tucson, 2005*
146. Shinohara S, Horii S *Jpn. J. Appl. Phys.* **46** 4276 (2007)
147. Gueroult R et al. *Plasma Sources Sci. Technol.* **25** 035024 (2016)
148. Liziakin G et al. *AIP Adv.* **7** 125108 (2017)
149. Liziakin G D et al. *Plasma Phys. Rep.* **48** 1251 (2022); *Fiz. Plazmy* **49** 278 (2023)
150. Antonov N et al. *Phys. Plasmas* **25** 123506 (2018)
151. Liziakin G et al. *J. Phys. D* **54** 414005 (2021)
152. Ahlfeld C et al., in *21st IEEE/NPS Symp. on Fusion Engineering SOFE 05, 26–29 September 2005, Knoxville, TN, USA* (Piscataway, NJ: IEEE, 2005) https://doi.org/10.1109/FUSION.2005.252859